

THESIS FOR THE DEGREE OF LICENTIATE OF ENGINEERING

Lipid-based liquid crystals as drug delivery vehicles  
for antimicrobial peptides

LUKAS BOGE



**CHALMERS**

Department of Chemistry and Chemical Engineering

CHALMERS UNIVERSITY OF TECHNOLOGY

Gothenburg, Sweden 2017

Lipid-based liquid crystals as drug delivery vehicles for antimicrobial peptides  
LUKAS BOGE

© LUKAS BOGE, 2017.

Licentiatuppsatser vid institutionen för kemi och kemiteknik  
Chalmers tekniska högskola  
Serie Nr: 2017:02  
ISSN: 1652-943X

Department of Chemistry and Chemical Engineering  
Chalmers University of Technology  
SE-412 96 Gothenburg  
Sweden  
Telephone + 46 (0)31-772 1000

Chalmers Reproservice  
Gothenburg, Sweden 2017

LUKAS BOGE

Department of Chemistry and Chemical engineering

CHALMERS UNIVERSITY OF TECHNOLOGY

### Abstract

The development of antimicrobial resistance is a great challenge within the health sector around the world. The demand for new efficient treatments is alarming in order to treat various bacterial infections in the near future. Antimicrobial peptides (AMPs) are a group of novel antibiotics that have gained more and more attraction the past decade. However, AMPs suffer from relatively low stability due to proteolytic and chemical degradation. As a consequence, carrier systems protecting the AMPs are highly needed for achieving efficient treatments. In this thesis, lyotropic liquid crystalline (LC) structures consisting of cubic glycerol monooleate/water and hexagonal glycerol monooleate/oleic acid/water have been examined as carriers for three AMPs (AP114, DPK-060 and LL-37). Both bulk gels and discrete dispersed structures, i.e. cubosomes and hexosomes have been studied. Moreover, two different peptide loading approaches for the cubosomes were tested and compared; pre- and post-loading. Characterization of the LC structures was performed using small-angle x-ray scattering (SAXS), dynamic light scattering,  $\zeta$ -potential, and cryogenic transmission electron microscopy (Cryo-TEM) and peptide loading efficacy by liquid chromatography. The antimicrobial effect of the AMP loaded LC nanoparticles (LCNPs) was studied *in vitro* using minimum inhibitory concentration (MIC) and time-kill assays. Proteolytic protection was investigated by incubating the formulations with two elastases and the antimicrobial effect after proteolysis was studied using radial diffusion assay (RDA).

Results showed that the most hydrophobic peptide (AP114) was prone to induce an increase in negative curvature of the bulk cubic LC gel, hence pushing the system towards a hexagonal structure. The most polar peptide (DPK-060) induced a decrease in negative curvature while LL-37 did not change the LC phase at all. The hexagonal LC phase was not affected by any of the AMPs. The cubic pre- and post-loaded LCNPs displayed promising antimicrobial activity, and sometimes a synergistic effect could be observed, resulting in a slightly better activity than the unformulated AMP. The hexagonal LCNPs were found to be very efficient in encapsulating the AMPs, but did not display any antimicrobial effect, indicating insufficient delivery of peptide to the bacteria. Moreover, cubosomes post-loaded with LL-37 were found to protect the peptide from proteolytic degradation, resulting in a significant better bactericidal effect after proteolysis.

**Keywords:** Liquid crystals, liquid crystalline nanoparticles, cubosome, hexosome, antimicrobial peptide, AMP, glycerol monooleate, proteolysis

## List of publications

1. Lipid-based liquid crystals as carriers for antimicrobial peptides: phase behavior and antimicrobial effect  
Lukas Boge, Helena Bysell, Lovisa Ringstad, David Wennman, Anita Umerska, Viviane Cassisa, Jonny Eriksson, Marie-Laure Joly-Guillou, Katarina Edwards and Martin Andersson  
*Langmuir*, 2016, 32, p. 4217–4228
2. Cubosomes post-loaded with antimicrobial peptides: characterization, bactericidal effect and proteolytic stability  
Lukas Boge, Anita Umerska, Nada Matougui, Helena Bysell, Lovisa Ringstad, Jonny Eriksson, Mina Davoudi, Katarina Edwards and Martin Andersson  
*Manuscript*

## Contribution report

1. Main author, responsible for all experimental work (except cryo-TEM imaging and *in vitro* bacterial effect studies), data evaluation and writing.
2. Main author, responsible for all experimental work (except cryo-TEM imaging and *in vitro* bacterial effect studies), data evaluation and writing.

## Publications not included in this thesis

1. Lipid-based nanoformulations for peptide delivery  
Nada Matougui, Lukas Boge, Anne-Claire Groo, Anita Umerska, Lovisa Ringstad, Helena Bysell and Patrick Saulnier  
*Int. J. Pharm.*, 2016, 502, p. 80-97

## Acknowledgement

My excellent supervisor **Martin Andersson**, for your engagement in this project and for your many clever ideas. You have really helped me to push this research to a higher level. My co-supervisors **Helena Bysell** and **Lovisa Ringstad**, for always being around, and for your support. Thank you all for your time!

**Anders Palmqvist**, for being my examiner and for your input regarding this work

*I would also like to thank:*

**Nada Matougui**, for help with HPLC, preparing bacteria for SEM and for being a wonderful host during my visit at the lab in Angers

**Anita Umerska** and **Viviane Cassisa**, for performing *in vitro* bacterial studies and for always being open for my strange ideas

**David Wennman**, for making very accurate peptide quantifications possible with UPLC

**Jonny Eriksson** and **Katarina Edwards**, for taking awesome cryo-TEM images of my particles and for valuable interpretation of the images

**Mina Davoudi**, for performing proteolysis and effect studies

**Romain Mallet** and **Florence Manero** for assistance during SEM-imaging of bacteria during my visit in Angers.

**Linnéa Nilebäck**, for assistance during plate reader measurements and fruitful discussions

**Lise-Britt Wahlberg**, for performing CD measurements

**Szymon Sollami-Delekta**, for fine tuning the preparation protocol for hexosomes and for help during the long night shift at MAXIV

People involved in the **FORMAMP-project**, for valuable discussions and input during the years

All personnel at **SP Kemi, Material och Ytor** for many interesting “fika” discussions and for support when labwork constantly fails ☺

**The MAX IV Laboratory**, for beam time at X-ray Synchrotron Beamline I911-SAXS

**Anand Kumar Rajasekharan**, for running part of the SAXS samples

The research performed in this study was funded by the European Union’s Seventh Framework Programme (FP7/2007-2013), under Grant Agreement No. 604182 within the **FORMAMP project**.

*“Vem är den där Kristallina Faser egentligen!?”-Tilda*

## List of abbreviations

AMP	Antimicrobial peptide
CFU	Colony forming units
Cryo-TEM	Cryogenic transmission electron microscopy
DLS	Dynamic light scattering
EC	Escherichia coli
GMO	Glycerol monooleate
HNE	Human neutrophil elastase
HPLC	High performance liquid chromatography
LC	Liquid crystal/liquid crystalline
LCNP	Liquid crystalline nanoparticle
MIC	Minimum inhibitory concentration
MRSA	Methicillin-resistant Staphylococcus aureus
OA	Oleic acid
PA	Pseudomonas aeruginosa
PE	Pseudomonas aeruginosa elastase
RDA	Radial diffusion assay
SA	Staphylococcus aureus
SAXS	Small angle x-ray scattering
SEM	Scanning electron microscopy
UPLC	Ultra performance liquid chromatography

## Table of Contents:

Abstract.....	III
List of publications.....	IV
Acknowledgement.....	V
List of abbreviations.....	VI
1. Introduction.....	1
1.1. Aim of this thesis.....	1
1.2. Background.....	2
1.2.1. Antimicrobial peptides.....	2
1.2.2. Antimicrobial peptides in this thesis.....	3
1.2.3. Lipid-based liquid crystals in drug delivery.....	4
1.2.4. Liquid crystalline nanoparticles in drug delivery.....	5
2. Experimental.....	7
2.1. Materials.....	7
2.2. Sample preparation.....	7
2.2.1. Liquid crystalline bulk gels.....	7
2.2.2. Liquid crystalline nanoparticles.....	7
2.3. Analytical methods.....	8
2.3.1. Particle size measurements.....	8
2.3.2. Zeta-potential.....	8
2.3.3. Small angle x-ray scattering.....	8
2.3.4. Quantification of encapsulated antimicrobial peptide.....	8
2.3.5. Release of antimicrobial peptide.....	9
2.3.6. Cryogenic transmission electron microscopy.....	9
2.3.7. Circular dichroism.....	9
2.4. In vitro studies.....	9
2.4.1. Microorganisms.....	9
2.4.2. Minimum inhibitory concentration.....	9
2.4.3. Time-kill assay.....	10
2.4.4. Proteolysis.....	10
2.4.5. Radial diffusion assay.....	10
2.4.6. Visualization of cells using scanning electron microscopy.....	11
3. Results and discussion.....	12

3.1.	Phase behavior of antimicrobial peptide loaded liquid crystalline gels .....	12
3.2.	Antimicrobial peptide loaded liquid crystalline nanoparticles .....	14
3.3.	In vitro antibacterial effect .....	21
3.4.	Proteolytic stability of post-loaded cubosomes .....	25
4.	Conclusions .....	27
5.	Future perspectives .....	28
6.	References .....	29

# 1. Introduction

The development of antimicrobial resistance of pathogenic bacteria is a great challenge within the health sector, all around the world. Estimations point out that up to 70% of the hospital acquired infections in the United States are caused by bacteria resistant to one or more antibiotics [1]. Since the discovery and deployment of penicillin in the 1940's, bacteria have developed resistance to all new types of antibiotics, in some cases just after a few years of use. In the past 40 years no new classes of antibiotics used clinically has been discovered, except two types of narrow spectrum drugs. Moreover, antimicrobial resistance is listed as one of the biggest threats to global health and development by the World Health Organization (WHO) and high rates of resistance development is observed over the planet. In the latest WHO report "*Antimicrobial resistance: global report on surveillance*" (2014) it was found that >50% of the bacteria commonly causing infections in hospitals and in the community (e.g. *Escherichia coli* and *Staphylococcus aureus*) had a reduced susceptibility to commonly used antibiotic treatments [2].

The demand for new efficient treatments is apparently alarming. It is doubtless a must in order to be able to treat various bacterial infections, large or small, in the future. A group of novel antimicrobial agents that has gained a lot of attraction since the early 1980's are antimicrobial peptides (AMPs) [3]. These peptides generally display a very quick, and usually broad spectrum, bacterial killing among being said to be less prone to develop high level resistance [3, 4]. AMP's common susceptibility to chemical and proteolytic degradation has limit AMPs in clinical use, but may be overcome by clever formulation strategies [5]. This thesis describes the use of liquid crystalline phases, and dispersions of those into nanoparticles, for delivery of AMPs.

## 1.1. Aim of this thesis

The aim of this thesis was to evaluate how three AMPs influenced the structure of cubic and hexagonal LC gel, and to study the suitability of LCNPs as drug delivery vehicles. Two different AMP loading approaches were investigated, presented in Figure 1, and compared, namely:

- a) Pre-loading , where AMPs are incorporated into the LC gel prior dispersion into LCNPs
- b) Post-loading, where the AMPs are let to associate onto pre-formed LCNPs

The antimicrobial effect of the AMP loaded LCNPs was studied *in vitro*, in order to reveal if the formulations could preserve, or even enhance the antimicrobial activity. It was also investigated if the particles could protect the AMPs from enzymatic degradation, and if any antimicrobial effect still was present after proteolysis.

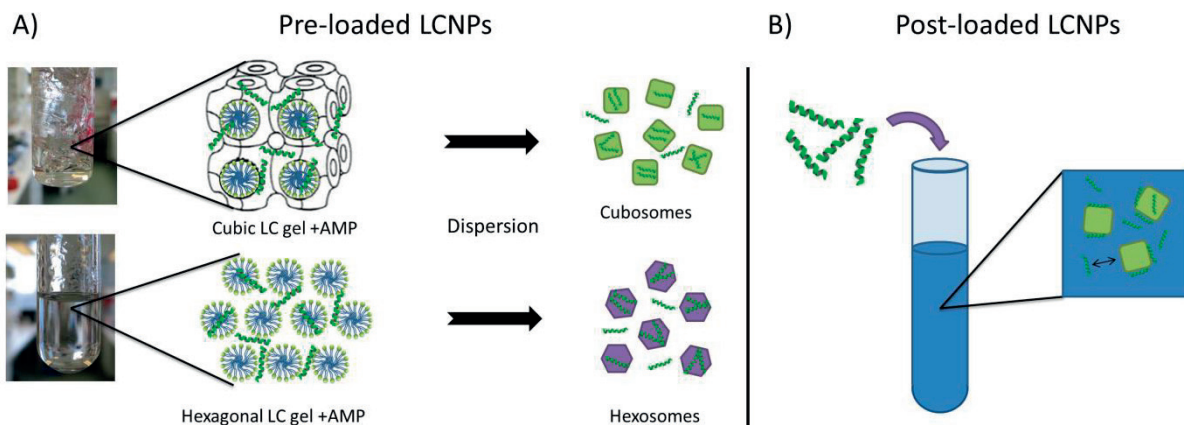


**Figure 1.** Schematical representation of the two AMP loading strategies investigated in this thesis; A) dispersion of LC gels pre-loaded with AMP, and B) where AMPs are let to associate onto LCNPs after preparation of the particles.

## 1.2. Background

### 1.2.1. Antimicrobial peptides

AMPs are present in all organisms as part of the innate defense system, thus making up the body's first response towards pathogenic bacteria. These peptides are promising therapeutics to treat various infectious diseases, due to their fast and non-specific mechanism of action [3, 4]. Bacteria are often said to be less prone to develop resistance against AMPs compared to traditionally used antibiotics. However, it has been shown that bacteria may develop resistance against AMPs and this issue needs to be carefully studied before translation into clinics [6]. AMPs are generally amphipathic molecules consisting of <45 amino acids, of which a substantial fraction are normally hydrophobic residues, and carries a net positive charge [7]. The positive net charge of the AMPs is an important property, driving the adsorption towards the negatively charged phospholipid head groups of the bacterial outer membrane, making strong interactions and penetration possible. There are several models as illustrated in Figure 2, describing the mode of action of AMPs, involving the barrel-stave, carpet and toroidal pore models [3]. All these models have in common that the AMP results in the formation of pores/defects within the bacterial membrane, leading to cell wall rupture and finally death.

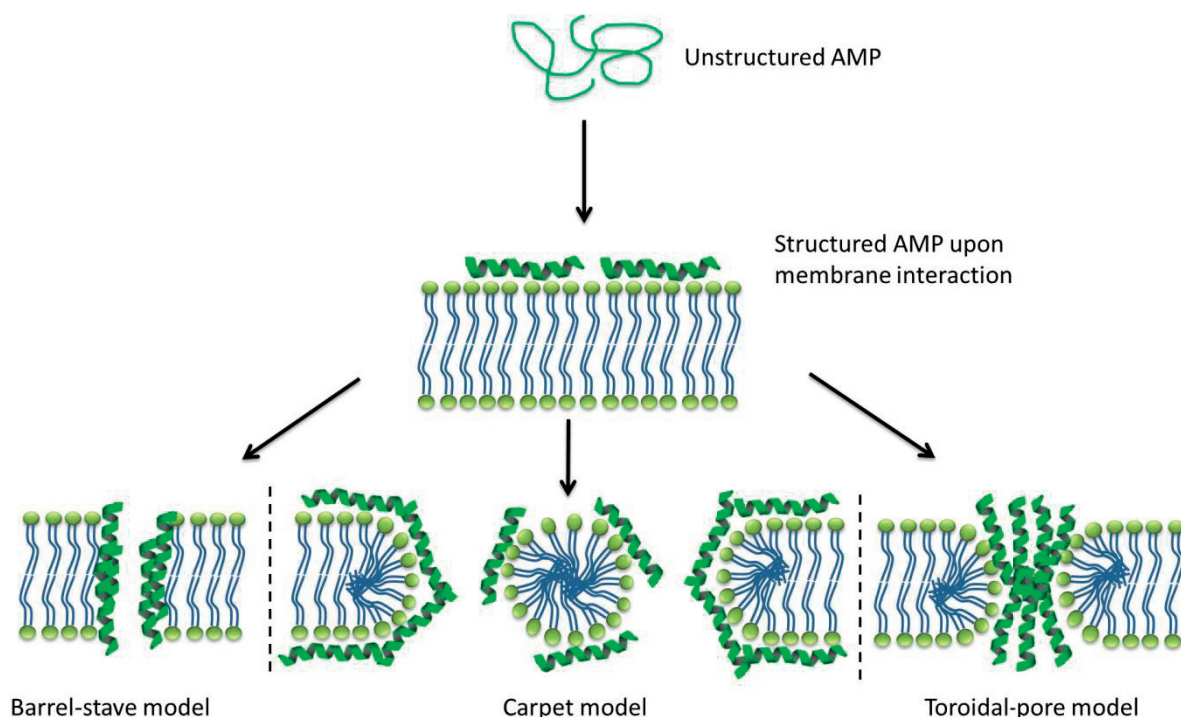


**Figure 2.** Models commonly used for describing the mechanism of killing bacteria by AMPs. AMPs are usually unstructured in aqueous solutions and change conformation upon adsorption and insertion in a bacterial membrane. If the AMP targets internal receptors of the cell, translocation through the membrane into the cytoplasm can also occur (not shown in illustration).

### 1.2.2. Antimicrobial peptides in this thesis

Three AMPs with differences in terms of size, charge, hydrophobicity, secondary structure and activity were chosen to study in this thesis. Peptide AP114 (also known as NZ2114) is a plectasin derivative derived from the fungus *Pseudoplectania nigrella* (“ebony cup” or “svart vårsål”), and kills bacteria by translocation through the bacterial membrane and inhibiting the membrane biosynthesis, through targeting of the cellular precursor Lipid II [8, 9]. Hence, the mechanism of action for AP114 differs from the more traditional killing models. The broad-spectrum antimicrobial peptide DPK-060 (also known as GKH17-WWW) is derived from the endogenous human protein kininogen [10]. The peptide is intended for topical administration to treat a variety of infected skin conditions [10]. Its effect has been confirmed by clinical phase II studies as treatment for infections in atopic dermatitis and acute external otitis [5]. LL-37 is the only known human peptide in the cathelicidin family, also showing a broad spectrum bacterial killing [11]. Its secondary structure normally changes from random coil in aqueous environment to  $\alpha$ -helix upon membrane interaction. The peptide is sensitive to proteolytic degradation by enzymes, which has so far limited its therapeutic use [12]. Table 1 summarizes the properties of the AMPs.

**Table 1. Properties of the antimicrobial peptides used in the thesis.**

Peptide	Sequence	MW	% hydrophobic AA	Net charge (pH 5.5)	Secondary structure	Antibacterial activity
AP114	GFGCNGPWNEDDLRCNHCKSI-KGYKGGYCAKGGFVCKCY	4411	40	+4.6	$\beta$ -sheet, $\alpha$ -helix	Gram-positive
DPK-060	GKHKNKGKKNKGKHNKWKWWW	2503	20	+8.5	Random coil	Broad spectrum
LL-37	LLGDFFRKSKEKIGKEFKRIVQR- IKDFLRNLVPRTES	4491	35	+6.3	$\alpha$ -helix, random coil	Broad spectrum

### 1.2.3. Lipid-based liquid crystals in drug delivery

LC phases are formed spontaneously upon hydration of certain amphiphilic molecules, e.g. polar lipids. The driving force for this self-assembly process of polar lipids into LC phases is the phenomenon often referred to as the “hydrophobic effect” [13, 14]. There are three main types of LC phases: the lamellar phase, the hexagonal phase and cubic phases with very complex 3-dimensional architectures. The LC phases are schematically presented in Figure 3 below.

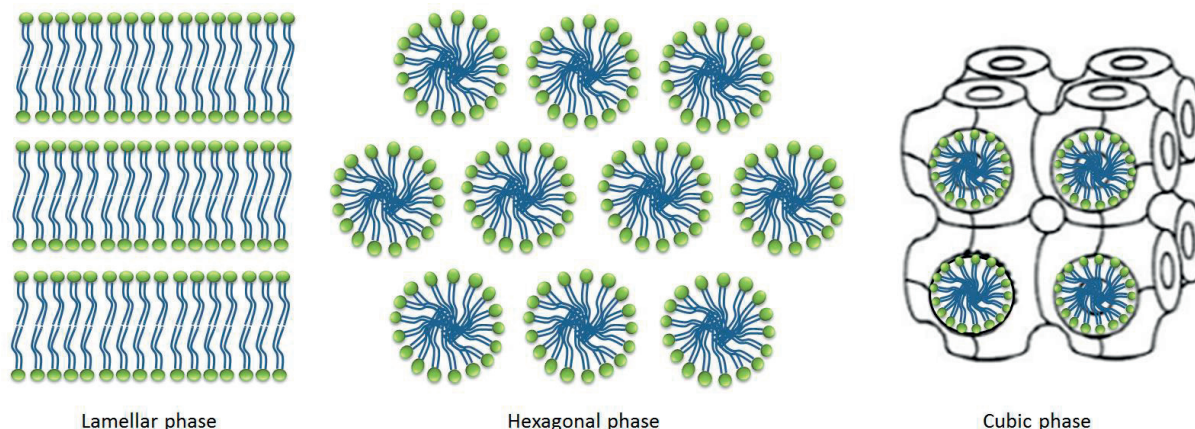


**Figure 3.** Schematically representation of the three major groups of liquid crystals; lamellar, hexagonal and cubic phase.

LC phases of polar lipids are of great interest in drug delivery because of their capability to encapsulate a broad range of drugs, ranging from hydrophobic to hydrophilic, as well as amphiphilic ones. Moreover, these systems are also biocompatible and degradable in the body [13]. One of the most extensively studied polar lipid in drug delivery is glycerol monooleate (GMO). GMO is known to have a very rich phase behavior with water, making room for many interesting drug delivery opportunities [15]. The water-GMO phase diagram is presented in Figure 4. Depending on the nature of the introduced guest molecules in such LC systems, e.g. the polarity and molecular structure, the molecules will be located either in the water or lipophilic domains of the system [16]. It has been shown that addition of lipophilic compounds to the GMO/water LC cubic system induce transition to a reverse hexagonal phase (increased negative curvature), while molecules having a pronounced amphiphilic character can induce transition to a lamellar LC phase (decreased negative curvature) [13, 17, 18]. AMPs comprising differences in amphiphilicity could be prone to induce similar phase transitions, when incorporated in such systems. Phase transitions have previously been shown for a variety of protein loaded LC systems [19-25]. In this work, the effect of incorporating three AMPs into a cubic and a hexagonal LC gel was studied.

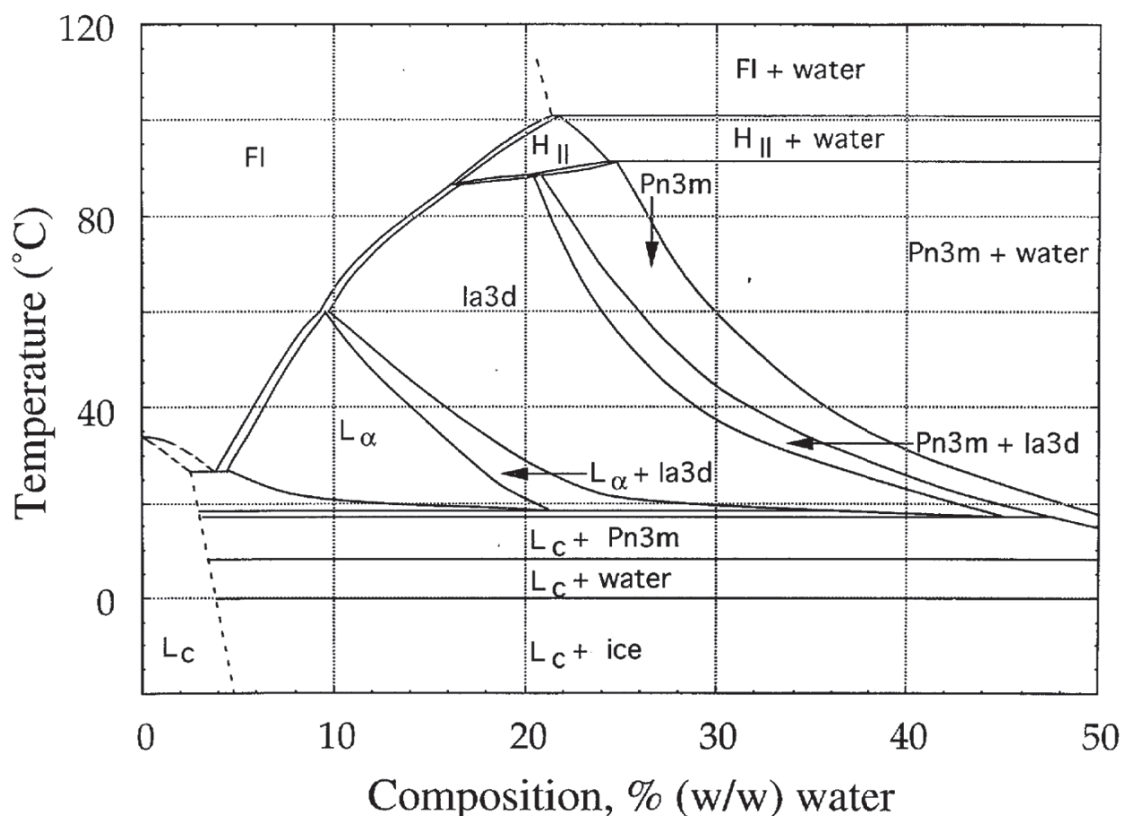


**Figure 4.** Water-GMO phase diagram displaying a rich variety of LC phases. The coexistence of LC phase and water enables fragmentation of bulk gel into LCNPs. Reprinted from [15], with permission from Elsevier.

#### 1.2.4. Liquid crystalline nanoparticles in drug delivery

One feature making LC systems of polar lipids even more interesting for drug delivery is the fact that some systems can coexist with excess of water. This enables fragmentation of bulk gels into LC nanoparticles (LCNPs), using a suitable stabilizer [26, 27]. A dispersion of cubic phase is commonly referred to as “cubosomes” while a dispersion of hexagonal phase is referred to as “hexosomes”. By doing this, one can overcome the usually sticky and highly viscous nature of the LC gels, which can be advantageous from a drug delivery perspective. Polar peptides and proteins can be incorporated in LCNPs and possibly be less subjected to chemical and proteolytic degradation [14, 28-30]. LCNPs can be prepared by sonication [27] or high pressure homogenizing using a microfluidizer [31] of bulk gel. Another preparation method involves dilution of an isotropic mixture of lipid and ethanol, commonly referred to as “the hydrotrope method” [32]. These preparation protocols have the drawback that they also produce a large fraction of vesicles among with the desired LCNPs (usually cubosomes or hexosomes) as can be revealed by cryo-TEM imaging. A way to reduce the number of vesicles is to heat treat the sonicated or microfluidized dispersions in an autoclave [33]. This treatment has several advantages, namely: 1) drastically reducing the number of small vesicles, 2) narrowing down the overall particle size distribution and 3) the final particle dispersion is sterile and suitable for pharmaceutical use.

Drug loaded LCNPs are typically obtained by adding the drugs either to the molten lipid phase (lipophilic drugs) or to the water phase (hydrophilic drugs) prior dispersion into

nanoparticles. However, peptide and protein drugs are often sensitive to high temperature, which may be induced by high shearing rates during fragmentation or during sterilization of the formulations. Hence, the number of preparation techniques for producing drug loaded LCNPs with high degree of uniformity is limited. One formulation strategy to form uniform drug containing LCNPs is to let a water soluble drug adsorb onto the surface of pre-formed heat treated LCNPs using electrostatic and/or hydrophobic interactions. This is possible since LCNPs usually have a slightly negatively zeta-potential, and would apparently attract antimicrobial peptides with a positive net charge. LCNPs have previously been investigated as carrier system for several peptides and proteins; insulin (pre-loading) [34], ovalbumin (pre-loading) [35-37], somatostatin (post-loading) [38] and cyclosporine A (pre-loading) [39, 40] only to mention a few. These studies report encouraging results in terms of observed blood glucose values (insulin, *in vivo*, rat), sustained release properties (ovalbumin, *in vivo*, rat), increased half-life time (somatostatin, *in vivo*, rat) and increased peptide skin penetration (cyclosporine A, *in vivo*, mice).

Taking the previously reported sustained release properties and protection against proteolytic degradation into account, makes LCNPs interesting drug delivery vehicles for a variety of peptides, such as AMPs.

## 2. Experimental

### 2.1. Materials

Glycerol monooleate (GMO) RYLO MG 19 Pharma was received from Danisco A/S (Grindsted, Denmark). The composition of the sample according to the manufacturer was min. 95% monoglyceride. The fatty acid content was minimum 88% oleoyl (C18:1). Super refined oleic acid NF-LQ-(MH) was purchased from Croda Inc. (Snaith, UK). The triblock copolymeric stabilizer Kolliphor® P407 poly(ethylene oxide)(PEO)-poly(propylene oxide)(PPO)-poly(ethylene oxide)(PEO) was obtained from BASF (Ludwigshafen, Germany) and had an approximate formula of  $\text{PEO}_{101}\text{PPO}_{56}\text{PEO}_{101}$  and an average molecular weight of 12600 g/mol. Antimicrobial peptide AP114 purity 99.1% was provided by Adenium Biotech ApS (Copenhagen, Denmark), DPK-060 (acetate salt) purity 98.5% (72.7% taking the acetate counter ion into account) was synthesized by Bachem AG (Bubendorf, Switzerland) and provided by Pergamum AB (Stockholm, Sweden) and LL-37 purity 94.7% was synthesized and provided by PolyPeptide Laboratories (Limhamn, Sweden).

### 2.2. Sample preparation

#### 2.2.1. Liquid crystalline bulk gels

LC gels were prepared by mixing melted GMO or GMO/OA (80:20 w/w) at 40 °C with a water solution containing AMP, resulting in LC gels containing 0.5, 1.0 and 1.5 w% peptide (if nothing else stated). Samples were homogenized with spatula, centrifuged at 3000 rpm for 1 hour and allowed to equilibrate at room temperature for at least 1 week prior further use. The lipid to water ratio for the LC gels prepared without AMP were chosen to obtain the cubic (70:30 w/w) or hexagonal phase (80:20 w/w), so the peptide's impact of the curvature could be investigated.

#### 2.2.2. Liquid crystalline nanoparticles

##### *Pre-loaded LCNPs*

Dispersions of the LC phases were made by fragmenting 5 w% (0.5 g) LC gel in 9.5 g 1.0% P407, dissolved in 5mM acetic acid buffer pH 5.5, using an Ultra-Turrax high shear mixer (IKA T25, Staufen, Germany) operated at 15.000 rpm for 1-2 min. The coarse dispersion was ultra-sonicated using a Vibra-Cell VC 750 (Sonics and Materials Inc., Newton, USA) equipped with a 6 mm probe operating at 40% of its maximum power in puls mode (3 s pulses followed by 7 break) for a total time of 5 min (cubic GMO dispersions) or 10 min (hexagonal GMO/OA dispersions).

##### *Post-loaded LCNPs*

Particles used for post-loading of AMP were prepared by dispersing a pre-formed cubic LC gel (GMO:water 70:30, no peptide added) as described above, followed by a heat treatment cycle of the sample, in order to narrow down the particle size distribution and to reduce the number of vesicles [33]. The heat treatment was done using a Laboklav 25 autoclave (SHP Steriltechnik AG, Schloss Detzel/Satuelle, Germany) at 121°C for 20 min. The final cubosome concentration was defined as the total dry content after the sterilization, in mg/mL of GMO+ P407, and quantified after removal of water through lyophilization (Epsilon 2-4

LSC plus, Martin Christ GmbH, Osterode am Harz, Germany) of the sample. Thereafter, samples containing 5 and 10 mg/mL cubosomes with AMP content of 0.10 mg/mL were prepared in 5 mM sodium acetate buffer pH 5.5. Two different concentrations of particles were chosen in order to investigate how it affected the peptide association. Samples were let to equilibrate for 24 hours at  $22 \pm 1^\circ\text{C}$  prior further analyses.

## **2.3. Analytical methods**

### **2.3.1. Particle size measurements**

The particle size and the particle size distribution of the LCNPs were measured by dynamic light scattering using a Zetasizer Zen3600 instrument (Malvern Instruments Ltd., Worcestershire, U.K.) using disposable cuvettes. Refractive indices were set to 1.47 and 1.33, for lipids and water respectively, and the temperature during the measurement was  $25^\circ\text{C}$  during the measurements. The hydrodynamic radius, assuming spherical particles, was calculated by the software using Stoke-Einstein's relation to describe the Brownian motion of the particles. Each sample was measured in triplicate.

### **2.3.2. Zeta-potential**

The zeta ( $\zeta$ ) -potential of the particles was determined by measuring the electrophoretic mobility using a Zetasizer Zen3600 (Malvern Instruments Ltd., Worcestershire, U.K.) using the Smoluchowski model. Samples were diluted in MilliQ water (pre-loaded particles) or in 5 mM sodium acetate buffer pH 5.5 (post-loaded particles) to a particle concentration of 1-2.5 mg/mL and analyzed in disposable measuring cells at  $25^\circ\text{C}$ . Each sample was run in triplicate.

### **2.3.3. Small angle x-ray scattering**

The LC structure of bulk gels and LCNPs was determined using SAXS. Measurements were performed at beamline I911-SAXS (MAX IV Laboratory, Lund, Sweden) equipped with a fast read-out pixel detector PILATUS 1M (Dectris Ltd., Baden, Switzerland) [41]. Liquid crystalline gels were mounted in a multiple sample holder made of steel and fitted between kapton sheets, whereas liquid samples were loaded into quartz capillaries (ID 1.0 mm) mounted in a steel holder. Samples were subjected to a flux of  $5 \cdot 10^{10}$  photons/s with a beam size of  $0.3 \times 0.3 \text{ mm}^2$  at a wavelength of  $0.91 \text{ \AA}$ . The exposure time was 100 s for each sample. Measurements were carried out in air at 22 and at  $37^\circ\text{C}$  for selected samples. Collected 2D raw-data images were analyzed using the software Bli911-4 GUI version 4.12 and the LC mesophases were identified according to Bragg peak spacing's [42].

### **2.3.4. Quantification of encapsulated antimicrobial peptide**

Liquid chromatography was used to quantify the encapsulated (pre-loaded particles) and cubosome-associated AMP (post-loaded particles). LCNPs were removed from the surrounding liquid by centrifugation at  $10\,000g$  for 30 min through Amicon Ultra-0.5 filter devices (Ultracel-100K, Merck Millipore Ltd. Corc, Ireland) with a 100 kDa molecular weight cut-off. The concentration of peptide in the filtrate was determined using UPLC or HPLC using a calibration curve and a correction factor compensating for adsorption to the filter. The amount peptide incorporated or associated to the LCNPs could then be calculated, as% of total added peptide. Details about the liquid chromatography instrumentation and methods can be found in Paper 1 and Paper 2.

### **2.3.5. Release of antimicrobial peptide**

Release of AMP from the post-loaded cubosomes was monitored through dialysis. 1 mL sample was placed in a Float-A-Lyzer® G2 dialysis device with 100 kDa molecular weight cut-off (Spectrum Laboratories Inc., Rancho Domingues, USA). Samples were let to dialyze in 12 mL 5 mM sodium acetate buffer pH 5.5, with or without 150 mM sodium chloride, at 22±1°C. A 200 µL sample was withdrawn after 0, 1, 2, 4, 6 and 24 h. The AMP release was quantified using a fluorescamine assay [43]. 180 µL of the samples was placed in a black 96-well plate and 20 µL 5 mg/mL fluorescamine (≥98%, Sigma Life Science, Saint Louis, USA) dissolved in acetone (99.9%, Sigma-Aldrich) was added to each well just prior fluorescent intensity measurement (excitation 360 nm and emission 465 nm) using a CLARIOstar® plate reader (GMB biotech, Ortenberg, Germany). Peptide quantification was performed using a standard curve.

### **2.3.6. Cryogenic transmission electron microscopy**

Cryo-TEM specimens were prepared in a controlled environment vitrification system kept at 25°C with humidity, close to saturation, to prevent evaporation from the sample during preparation. A droplet of the LCNP dispersion was placed onto a carbon-coated holey polymer film supported by a copper grid, gently blotted with a filter paper to form a thin liquid film (10-500 nm), and immediately plunged into liquid ethane at -180°C. The sample grid was then kept at liquid nitrogen temperature and transferred into a Zeiss LIBRA-120 transmission electron microscope (Carl Zeiss, Oberkochen, Germany) operated at 80kV in zero-loss bright-field mode. Digital images were recorded under low dose conditions with a TRS slow scan CCD camera system (TRS GmbH, Germany) and iTEM software (Olympus Soft Imaging Solutions GmbH, Germany). An underfocus of 1-3 µm was used in order to enhance contrast.

### **2.3.7. Circular dichroism**

Circular dichroism (CD) spectra were measured by a Jasco J-810 Spectropolarimeter (Jasco, Easton, USA). The measurements were performed at 37 °C in a 10 mm quartz cuvette under stirring. The samples (100 µg/mL AMP, 10 mg/mL cubosomes) were diluted 5 times with buffer prior analysis in order to get a good signal from the instrument. The effect on peptide secondary structure was monitored in the range 200–260 nm.

## **2.4. In vitro studies**

### **2.4.1. Microorganisms**

The bacteria used to characterize the antimicrobial activity of the AMP loaded LCNPs were *Staphylococcus aureus* (SA), reference strain ATCC 25923 and 29213, methicillin-resistant *Staphylococcus aureus* (MRSA) clinical strain No. 0702E0196, *Pseudomonas aeruginosa* (PA), reference strain ATCC 27853, ATCC PA01 and clinical strain No. 0704C0134, *Escherichia coli* (EC), reference strain ATCC 25922, and ESBL *E. coli*, clinical strain 9007550201, and *Acinetobacter baumannii*, AYE reference strain ATCC BAA-1710.

### **2.4.2. Minimum inhibitory concentration**

The antimicrobial activity of pure peptides and peptide loaded LCNPs was first screened using minimum inhibitory concentration (MIC). Serial two-fold dilutions of the tested AMP

loaded LCNP samples in brain heart infusion broth (BHI) (BioMérieux, France) for AP114 containing samples or 1% BHI in water for DPK-060 and LL-37 containing samples were prepared in order to obtain the desired concentration range. The density of the microorganism suspension was adjusted to 1.1 McFarland standard corresponding to approximately  $3.3 \cdot 10^8$  colony forming units (CFU)/mL (for *SA*) or to 0.5 McFarland, approximately  $1.5 \cdot 10^8$  CFU/mL (*PA*, *EC*, *A. baumannii*). The former suspensions were further diluted 100 times ( $3.3 \cdot 10^6$  CFU/mL), and the latter were diluted 10 times ( $1.5 \cdot 10^7$  CFU/mL) with BHI or 1% BHI in water. An aliquot of 100  $\mu$ L of the bacterial suspension was added into each well of a sterile 96 well plate containing 100  $\mu$ L of the tested sample. Positive controls containing only the medium and the bacterial suspension (growth control) and negative control wells, containing the medium and the tested sample without the bacterial suspension (sterility control), were also prepared. The plates were incubated at 37°C for 24 hours. The MIC was defined as the lowest concentration of the sample that completely inhibited the growth of the bacteria as detected by the unaided eye.

#### **2.4.3. Time-kill assay**

To evaluate the bactericidal activity of the samples, time-kill assays were performed. An amount of 20  $\mu$ L of the inoculum (prepared in BHI or 1% BHI in water) was added to a polypropylene tube containing 1.98 mL of the tested sample in BHI or 1% BHI. BHI or 1% BHI containing the bacterial suspension without the tested sample was used as positive control. The samples containing the tested LCNPs, as well as the controls were incubated at 37°C. At each sampling time (0, 3, 6 and 24 hours) an amount of 100  $\mu$ L was withdrawn from each tube. Serial 100-fold dilutions were prepared in distilled water when necessary. A 100  $\mu$ L aliquot of the diluted and/or undiluted sample was placed onto the surface of the agar and allowed to be absorbed into the agar. After incubation of the agar plates for 24 hours at 37°C, the colonies were counted and the cell density in CFU/mL could be calculated.

#### **2.4.4. Proteolysis**

The peptides and peptides post-loaded on cubosomes (2  $\mu$ g peptide) were incubated for 6 hours at 37°C with 0.2  $\mu$ g *Pseudomonas aeruginosa* elastase (PE) (261.0 units/mg, BioCol GmbH, Potsdam, Germany), or 0.4  $\mu$ g human neutrophil elastase (HNE) (20.0 units/mg, Calbiochem, La Jolla, USA) in a total volume of 15  $\mu$ L. The materials were analyzed on 10–20% precast Tris-Tricine sodium dodecyl sulfate polyacrylamide (SDS-PAGE) gels (Invitrogen) using electrophoresis and analyzed after staining with coomassie brilliant blue, in order to visualize peptide degradation.

#### **2.4.5. Radial diffusion assay**

Bacteria were grown to mid-logarithmic phase in 10 mL Todd Hewitt (TH) medium and washed once with 10 mM Tris buffer pH 7.4. An amount of  $4 \cdot 10^6$  CFU was added to 5 mL of the underlay agarose gel (consisting of 1% (w/v) low-electroendosmosis (Low-EEO) type agarose, 0.02% (v/v) Tween 20, and 0.03% trypticase soy broth (TSB) (w/v)). The underlay was poured into  $\varnothing$  85 mm petri dishes. Thereafter, 4 mm diameter wells were punched in the underlay gel, and 6  $\mu$ L of the samples were added to each well and the plates were incubated at 37°C for 3 hours. The underlay gel was then covered with 5ml of molten overlay gel (6% TSB and 1% Low-EEO agarose in water) and incubated at room temperature overnight. The

antimicrobial activity of samples was visualized as a clear zone around each well. The results from these experiments are given as mean diameters (n=4-5) of the clear zones formed for the different peptide samples.

#### **2.4.6. Visualization of cells using scanning electron microscopy**

In order to visualize the cell morphology after incubation with AMP loaded LCNPs, bacterial samples were prepared for scanning electron microscopy (SEM). The cells were incubated at the same cell concentrations as for the time-kill assays. After 9 hours incubation, cells were let to adsorb onto poly-L-lysine coated 1\*1 cm glass slides for 1 hour, resulting in a total incubation of 10 hours. The bacteria suspension was thereafter gently aspirated and replaced by fresh phosphate buffered saline (PBS) pH 7.4 twice. Then, fixative solution (2% glutaraldehyde and 2% paraformaldehyde in PBS) was added and left overnight at room temperature. Following day, samples were rinsed with PBS and dehydrated using an ethanol series and thereafter desiccated using hexamethyldisilazane:ethanol 1:1, 1:0 (45 min in each solution, last step done twice) and let dry overnight in a fume hood. Samples were sputtered with platinum and transferred into the microscope. Cells were imaged using a Jeol JSM-6301F scanning microscope (JEOL Ltd, Japan) operated at 3 kV.

### 3. Results and discussion

In this section results are presented with the intention to make comparisons between the two LC delivery systems, the cubic GMO/water and the hexagonal GMO/OA/water, and between the two different peptide loading approaches for the LCNPs: pre- and post-loading. The pre-loaded LC systems are discussed in Paper 1, while the data from the post-loaded systems are presented in Paper 2.

#### 3.1. Phase behavior of antimicrobial peptide loaded liquid crystalline gels

The effect of incorporating AMPs into cubic and hexagonal LC gels was studied using SAXS, and diffractograms are presented in Figure 5. As can be seen in the diffractograms for the cubic GMO-based gels, the LC structure was kept for LL-37, changed to another cubic symmetry in case of DPK-060 or gradually turned into a hexagonal phase in case of AP114. The LC structure of the hexagonal gels was unchanged upon incorporation of any of the AMPs at the studied concentrations, and was thus found to be more robust upon peptide addition. Lattice parameter calculations are presented in Paper 1. The reference cubic gel (no peptide added) belonged to the Ia3d space group, with a lattice parameter of 141.3 Å, in agreement with phase diagrams found in literature at 30% water content [15, 44]. When the AP114 peptide was added to the system, having the highest percentage of hydrophobic residues and lowest net charge among the tested AMPs, the structure gradually turned into the hexagonal phase. Hence, AP114 is suggested to interact strongly with the hydrophobic parts of the GMO membranes, thus increasing the critical packing parameter (CPP), and in turn increasing the negative curvature. Interestingly, the cubic Pn3m phase was detected at lower peptide additions, representing a decrease in negative curvature. Transitions from Ia3d to Pn3m, and also further to H<sub>2</sub>, has previously been observed for lipophilic molecules or amphiphilic peptides added to GMO based systems [45]. As seen for AP114 at low concentrations, DPK-060 changed the structure from cubic Ia3d to cubic Pn3m above 0.5% peptide addition. This is probably a result of DPK-060 being the most hydrophilic peptide among the examined AMPs and with highest charge. DPK-060 is believed to interact strongly with the hydrophilic head groups of GMO, resulting in a decreased CPP and in turn the negative curvature. LL-37 did not affect the cubic Ia3d structure, indicating that the peptide is mostly located in the water domains of the structure or is penetrating the bilayer interfaces without significantly changing the curvature.

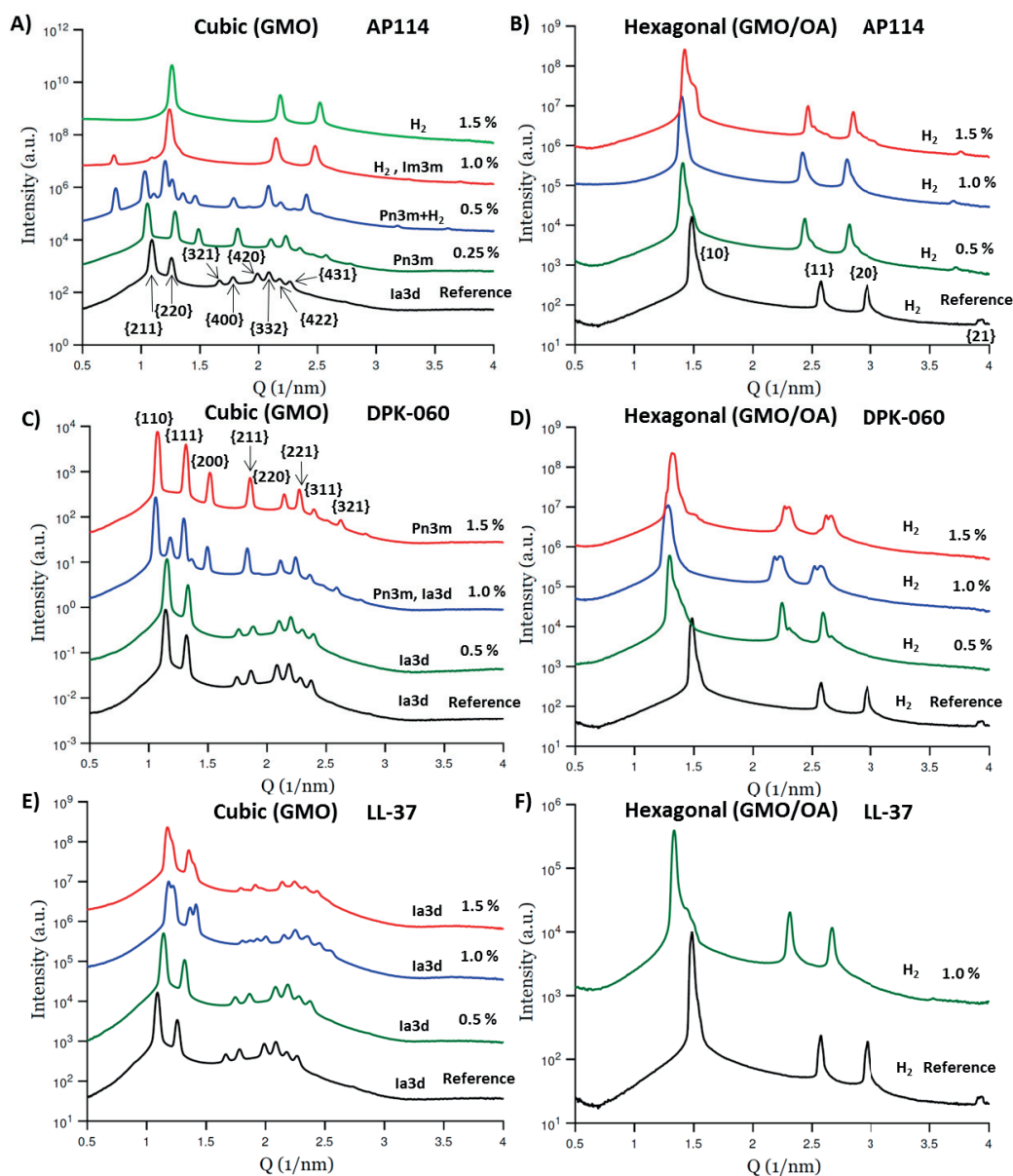


**Figure 5.** SAXS diffractograms of cubic GMO:water 70:30 w/w% (A, C, and E) and hexagonal GMO/OA:water 64:16:20 w/w/w% (B, D and F) LC gels containing AMPs AP114, DPK-060 and LL-37 at different concentrations (w%). Representative peak indexing for the cubic Ia3d (A), hexagonal (B) and cubic Pn3m (C) symmetries are displayed as the corresponding Miller indices [hkl].

As mentioned earlier, the hexagonal GMO/OA gels kept their LC structure upon peptide addition. However, the lattice parameter for the H<sub>2</sub> phase without AMP (48.9 Å) was found to increase, represented by the shift of peaks to lower q-values, when any of the AMPs were introduced. The observed increase in lattice parameter indicates a swelling of the structure. The most hydrophobic peptide, AP114, showed the smallest increase in lattice parameter. The reason for this could be that the peptide is mostly located in the lipophilic parts of the structure, thus increasing the bulkiness and length of the hydrophobic tails, without changing the radius of the water channels. The greatest swelling was observed for DPK-060. Due to its high positive net charge and hydrophilicity, DPK-060 is most prone to interact with the polar head groups and water domains in the hexagonal structure, thus swelling the cylinders

diameter resulting in an increased lattice parameter. Moreover, electrostatic repulsion between the positive charges of the AMPs could play a role in the increase of the lattice parameter.

### 3.2. Antimicrobial peptide loaded liquid crystalline nanoparticles

Two different peptide loading approaches were investigated for LCNPs in this work: pre-loading and post-loading, as previously described in Figure 1. For the pre-loaded LCNPs (GMO and GMO/OA-based), the AMPs were added in the LC gel before dispersion into nanoparticles using high-shear mixing followed by ultra-sonication. The particles used for post-loading (GMO-based cubosomes) were prepared in the same way, but with no AMP incorporated in the LC gel from the start, with an additional heat-treatment cycle in an autoclave. This treatment is known to narrow down the particle size distribution and to fuse smaller vesicles together to cubosomes, or sometimes to larger vesicles. The difference in particle size distributions and particle morphology between pre- and post-loaded GMO-based particles is presented in Figure 6. The ultra-sonicated particles had a mean particle size of 127 nm with a polydispersity index (PDI) of 0.140, compared to after heat treatment 192 nm with PDI of only 0.050. A clear reduction of the number of small vesicles was observed after the heat-treatment, as expected. Only GMO-based cubosomes were selected to investigate in post-loading approach. This was due to difficulties retaining the hexagonal LC symmetry of the particles upon autoclavation of the GMO/OA system, as revealed by SAXS (unpublished data). Moreover, the hexagonal LCNPs did not show any antimicrobial activity (section 3.3) and was therefore excluded.

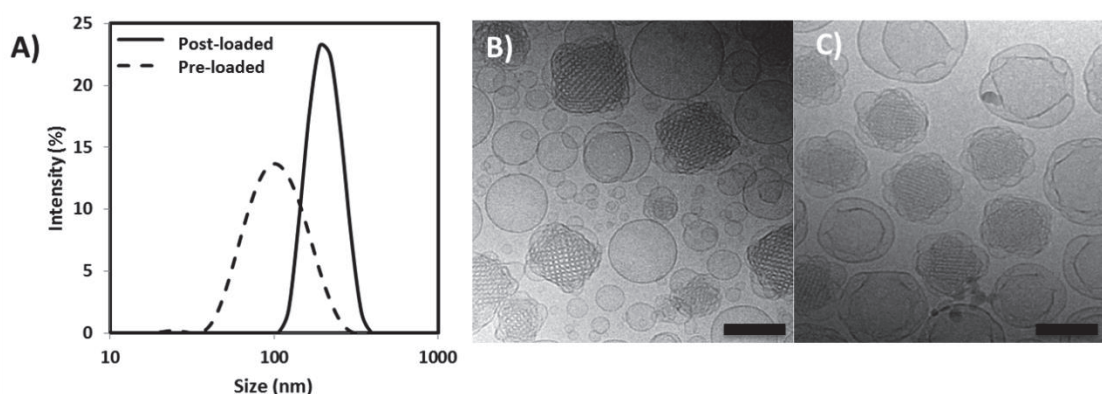


**Figure 6.** Particle size distributions for GMO-based pre-loaded particles (ultra-sonicated) and post-loaded particles (ultra-sonication followed by autoclavation) measured by DLS (A). Representative cryo-TEM images of pre-loaded particles (B) and post-loaded particles (C), without any AMP, displaying differences in content of small unilamellar vesicles. Scale bar equals 100 nm.

The internal LC structure of the pre- and post-loaded LCNPs were determined using SAXS and diffractograms are presented in Figure 7. It was found that the GMO-based pre-loaded particles (Figure 7 A, C and E) belonged to the Im3m cubic symmetry, displaying 3 characteristic Bragg peaks with spacing's of  $2^{1/2}$ :  $4^{1/2}$ :  $6^{1/2}$ . Interestingly, AP114 containing samples displayed hexagonal structure at 1.0 w% peptide loading at 37 °C and at 1.5 w% at 22 °C, in agreement with the hexagonal phase found in the LC bulk gels. Samples containing DPK-060 and LL-37 did always display cubic Im3m phase. The GMO/OA-based LCNPs (Figure 7 B, D and F) displayed presence of hexagonal structure by the 3 peaks with spacing's of  $1^{1/2}$ :  $3^{1/2}$ :  $4^{1/2}$ , in agreement with the results from undispersed gels.

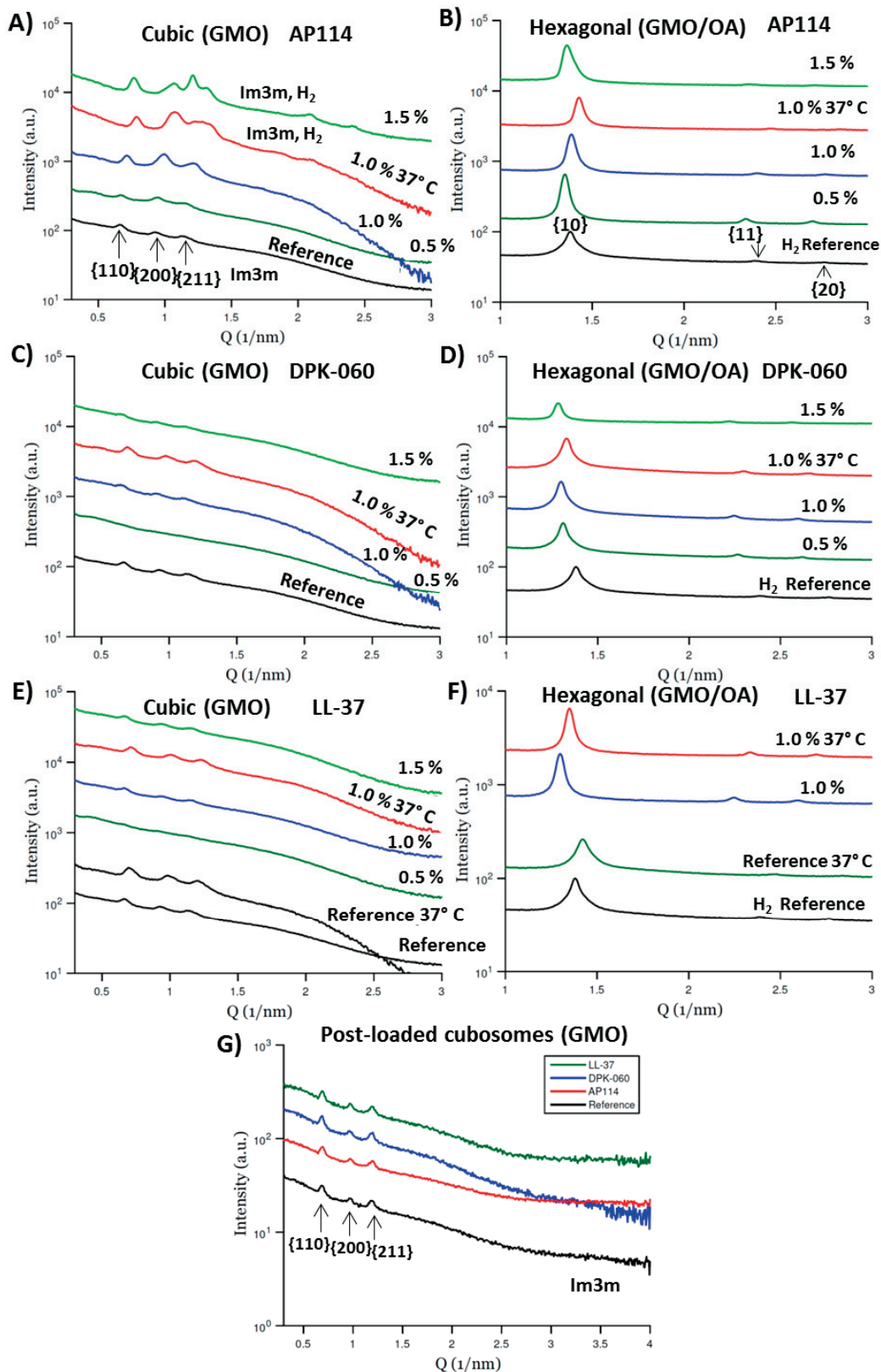


**Figure 7.** SAXS diffractograms of pre-loaded LCNPs (A-F) and post-loaded cubosomes (G). The peptide loading in% reflects the initial peptide content in the undispersed LC gel for the pre-loaded particles (A-F). The particle concentration for the post-loaded cubosomes was 10 mg/mL and peptide concentration 0.10 mg/mL. Representative peak indexing for the cubic Im3m (A and G) and hexagonal (B) symmetries are displayed as the corresponding Miller Indices [hkl].

The LC structure of the post-loaded cubosomes was also found to belong to the Im3m cubic symmetry, and no apparent difference was observed upon peptide addition (Figure 7 G). This may indicate that the AMPs are not migrating deeper inside the lipid particles, as we do not observe any phase transition e.g. for AP114 in this case, compared to pre-loaded AP114 (Figure 7 A) displaying presence of hexagonal phase.

Furthermore, the LCNP dispersions were characterized in terms of particle size,  $\zeta$ -potential and peptide loading efficacy. Results for the pre-loaded cubic GMO and hexagonal GMO/OA particles are illustrated in Figure 8. For the cubic LCNPs, the mean particle size was always in the range of 100-130 nm with a particle size distribution PDI <0.160. The mean particle size for the hexagonal LCNPs was in the range 140-170 nm and showed slightly broader distributions of particles (PDI<0.220). In general, pre-loaded GMO-based particles showed lower peptide loading efficacies (41-86%), compared to dispersions of GMO/OA hexagonal LC gels (>94%). Different trends in loading efficacy were observed for the peptides loaded in the cubic LCNP. No clear trends were observed for the hexagonal GMO/OA system. The  $\zeta$ -potential for the pre-loaded references (no AMP added) particles were always negative and increased upon peptide incorporation, indicating presence of peptide on the particle surfaces.

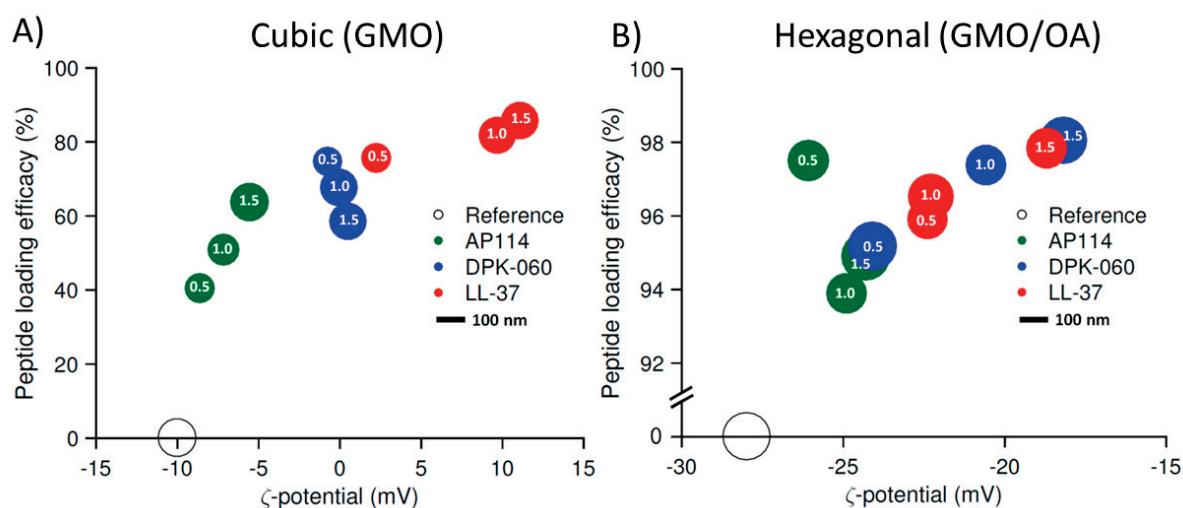


**Figure 8.** Peptide loading efficacy plotted as function of  $\zeta$ -potential, for pre-loaded cubic (A) and hexagonal (B) LCNPs. The diameter of the bubbles is proportional against its mean particle size. The cubic reference equals 127 nm and the hexagonal 159 nm (unfilled circles). Numbers inside circles represent initial peptide loading (w%) in dispersed gels.

Peptide association onto post-loaded cubosomes was quantified by liquid chromatography measurements (Figure 9 A), followed by peptide concentration scans in  $\zeta$ -potential (Figure 9 B) and circular dichroism (Figure 9 C). The same trends in peptide encapsulation efficacy (AP114<DPK-060<LL-37) seen for the pre-loaded cubic particles, were also observed for the post-loaded systems. Peptide located at the cubosome surface was studied at two different particle concentrations, 5 and 10 mg/mL, at a fixed peptide concentration of 0.10 mg/mL. Samples containing 5 mg/mL particles showed only 7-8% association of the peptides AP114 and DPK-060. If the concentration of cubosomes was doubled (from 5 to 10 mg/mL AMP association to the particles more than doubled, for those two peptides. Interestingly, LL-37 with properties in between AP114 and DPK-060 in terms of hydrophobicity and net charge,

showed a much higher degree of association (>60%) independent of the particle concentration. The properties of AP114 having a low positive net charge (+4.6), large fraction hydrophobic residues (40%) and high molecular weight (4411 g/mole), did not favor a strong association onto the particles. The drastic increase of cubosome-associated AP114 and DPK-060 when particle concentration was doubled indicates a sensitive equilibrium between adsorbed and non-adsorbed peptide, which opens up for triggered release opportunities. One could believe that the electrostatic interactions would be the most important factor influencing the peptide association to cubosomes. However this hypothesis does not hold in case of DPK-060 (+8.5), that comprises the highest positive net charge, but still showed lower adsorption compared to LL-37 (+6.3). Hence, the peptide's hydrophobicity and molecular weight does most likely also play a role in the adsorption process. The presence of the positively charged AMPs onto cubosomes outer surface was further indicated by the increase in  $\zeta$ -potential upon peptide addition, as displayed in Figure 9 B. Peptide LL-37 showed largest change in  $\zeta$ -potential, compared to DPK-060 and AP114 showing smaller changes, in good agreement with the trends of liquid chromatography data. The  $\zeta$ -potential was always slightly negative (in absolute values) at lowest peptide concentrations and turned positive at higher concentrations.

CD measurements were performed on post-loaded cubosomes in order to detect any changes in peptide secondary structure upon association to the cubosome particles (Figure 9 C). None of the pure AMPs displayed any clear signs of secondary structure and were most likely in a random coil conformation. Results for AP114 and LL-37 showed a change in CD spectra with two minima approximately at 210 nm and 225 nm, characteristic for a transition into  $\alpha$ -helical structure in the presence of the cubosomes particles. These findings further indicate that peptide association to the cubosome particles takes place. Pure AP114 was expected to display presence of  $\beta$ -sheet structure as well, but no clear minima around 215 nm could be observed. The transition from a more unordered structure to more helical upon interaction of LL-37 with cubosomes, is in good agreement with data reported previously, also displaying increase in  $\alpha$ -helicity upon membrane adsorption and vesicle interaction [11, 46].

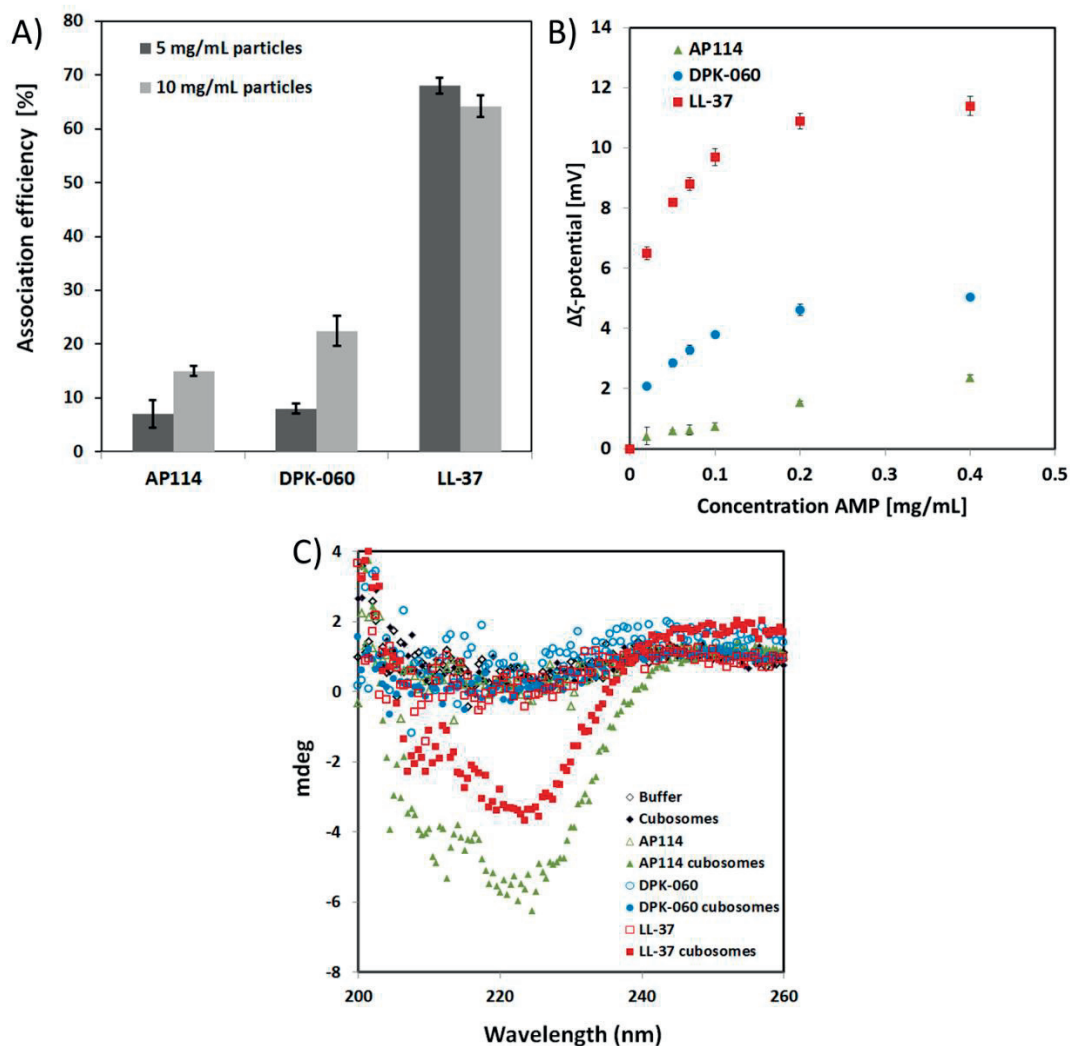


**Figure 9.** Peptide association efficacy for post-loaded cubosomes (A), peptide association to cubosomes monitored as change in  $\zeta$ -potential (B) and peptide secondary structure measured by CD (C), indicating adsorption of peptides on the particle surfaces. Cubosome concentration was 1 mg/mL in the  $\zeta$ -potential scan and 2 mg/mL for CD in order to get a good signal from the instruments. The peptide concentration was 20  $\mu$ g/mL for the CD measurements. Data is presented as mean values  $\pm$  standard deviation ( $n=3$ ) in diagram A and B.

Cryo-TEM images of both pre-loaded cubic and hexagonal dispersions as well as post-loaded cubosomes, presented in Figure 10, displayed a fraction of dense particles with internal structure, in line with the observed diffraction peaks revealed by SAXS. The cubosome particles did sometimes carry vesicle structures on the edges. On the other hand, the hexosome particles were found to be more round shaped, with a more blurry internal repeating structure. A clear reduction in the fraction of small unilamellar vesicles was observed for the post-loaded particles (Figure 10 I-L). This was expected, as a result of the heat-treatment of the particles prior to the addition of AMPs, in line with cryo-TEM images found in the literature [33]. Moreover, the particle size was found to be more homogenous, as revealed by the DLS-data presented in Figure 6 A. From Figure 10 A, the repeating distance in the cubosome particles was measured to approximately 90-95  $\text{\AA}$ , also in good agreement with the calculated d-spacing from the (110) reflection in the SAXS-data, found to be  $135/\sqrt{2} = 95.5 \text{ \AA}$ .

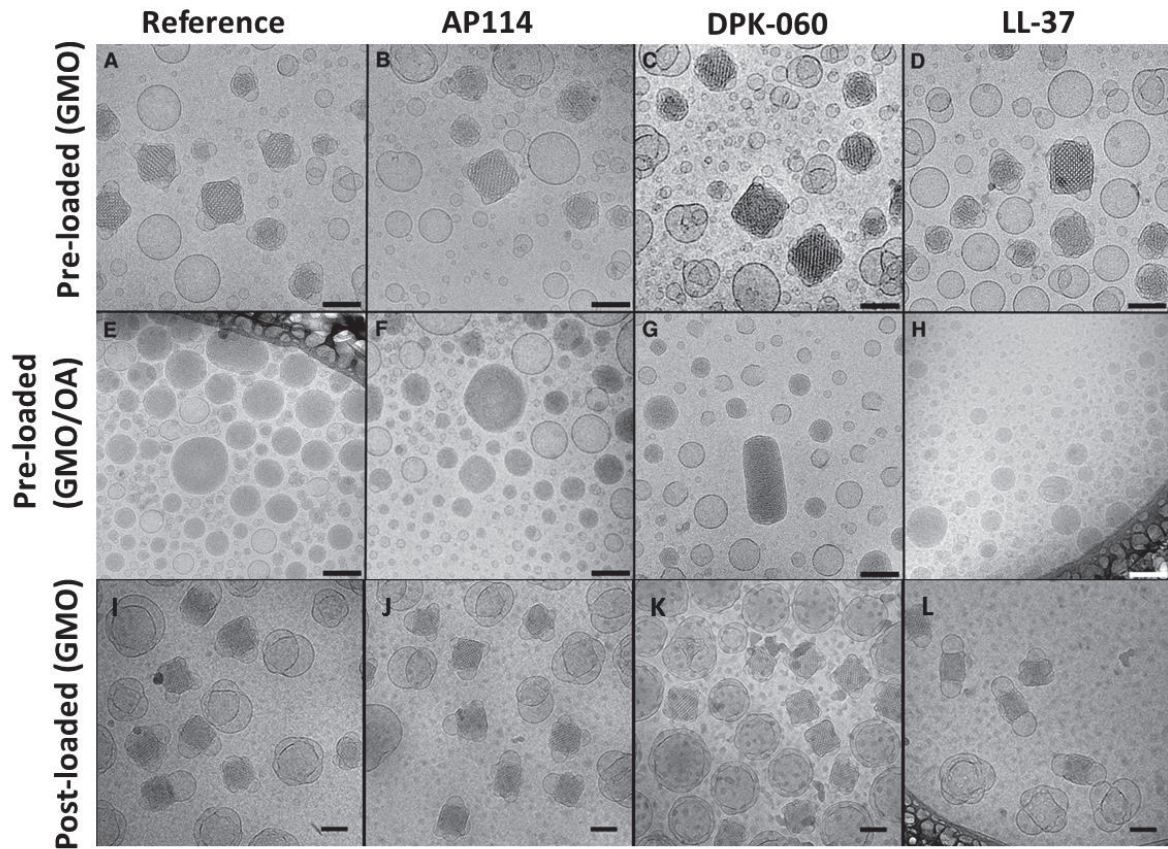


**Figure 10.** Cryo-TEM images of pre- and post-loaded LCNPs. Pre-loaded GMO-based (A-D) and GMO/OA-based (E-H) were loaded with 1 w% AMP prior dispersion resulting in a final concentration of 500  $\mu\text{g}/\text{mL}$ . Post-loaded GMO-based particles (I-L) contained 100  $\mu\text{g}/\text{mL}$  AMP at the higher particle content (10  $\text{mg}/\text{mL}$ ). Scale bar equals 100 nm.

The release of AMP from post-loaded cubosomes was monitored by dialysis in 5 mM sodium acetate buffer pH 5.5 with or without physiological salt concentration (150 mM NaCl). Results are presented in Figure 11 and show that the release of AP114, DPK-060 and LL-37 from the cubosomes particles was drastically reduced at higher ionic strength. These data are further interpreted in the next section (3.3) about the *in vitro* effect of the AMP loaded particles. Release from pre-loaded cubic and hexagonal LCNPs indicates that only the free (non-encapsulated peptide) was transferred over the dialysis membrane. This is due to the fact that the total amount of released peptide agrees perfectly with the peptide encapsulation efficacy, quantified by UPLC (unpublished data). Hence, one can hypothesize that the peptides like to take place in the LC structure, and are not prone to diffuse or leak out from the particles.

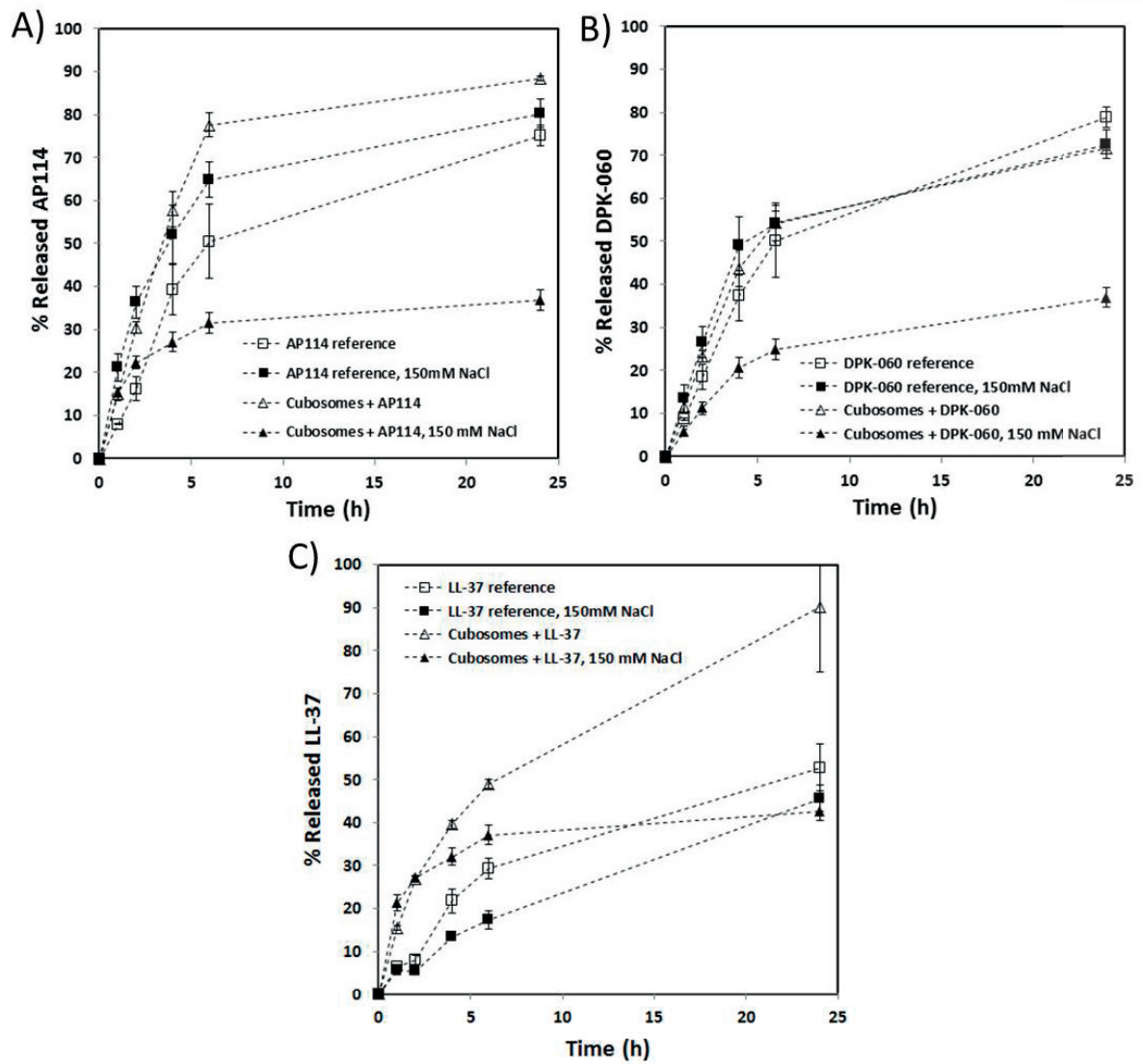


**Figure 11.** Release of AMP from post-loaded cubosomes including references with only AMP; AP114 (A), DPK-060 (B) and LL-37 (C). Each experiment was repeated twice. The release of AMPs from cubosomes appeared to be slower at higher ionic strength.

### 3.3. In vitro antibacterial effect

The first screening of the antimicrobial activity of the peptide-loaded LCNPs was done by minimum inhibitory concentration (MIC) tests using 7 different bacterial strains. MIC data is presented in Table 2, except for pre-loaded hexagonal GMO/OA particles which did not display any antimicrobial activity (MIC >16 µg/mL) for all tested strains. No apparent difference concerning the two different particle concentrations (i.e. 5 mg/mL and 10 mg/mL) was observed for the post-loaded cubosomes, and data for 10 mg/mL particles is therefore only shown.

**Table 2.** MIC values for unformulated peptide (UF) and for pre- and post-loaded GMO-based particles. Pre-loaded particles contained 500 µg/mL AMP and post-loaded 100 µg/mL. The hexagonal (GMO/OA) LCNPs did not display any antimicrobial activity at the tested concentrations (MIC >16 µg/mL) for all strains, and were therefore excluded in the table below.

<i>MIC values (µg/mL)</i>									
Bacterial strain	AP114			DPK-060			LL-37		
	UF	Pre (GMO)	Post (GMO)	UF	Pre (GMO)	Post (GMO)	UF	Pre (GMO)	Post (GMO)
<i>S. aureus</i>	8	8	8-16	4	2-4	1-2	8-16	>16	>16
MRSA	4	4	4	4	2-4	2	8-16	>16	>16
<i>P. aeruginosa</i>	-	-	-	8	16	8-16	8-16	>16	8-16
<i>P. aeruginosa</i> clinical strain	-	-	-	16	8-16	8	8-16	8	8-16
<i>E. coli</i>	-	-	-	8	2-4	4	16	16	8-16
ESBL <i>E. coli</i> clinical strain	-	-	-	4-8	2-4	2-4	16	>16	≥16
<i>A. Baumannii</i>	-	-	-	4-8	16	16	16	>16	≥16

In general, AP114 and DPK-060 loaded LCNPs did preserve the antimicrobial effect compared to unformulated peptide. LL-37 containing samples showed a slight reduction in its usually broad spectrum activity and were only active against gram negative strains. The reason for this could be that the peptide needs to be delivered in different ways for different bacteria in order to adsorb sufficient and penetrate the membrane. Interestingly, the activity for the pre- and post-loaded GMO particles gave very similar MIC values, even though the degree of encapsulated or cubosome-associated AMP were different (usually lower for the post-loaded). For example pre-loaded particles with DPK-060 with an encapsulation efficacy of over 60% performed as well as post-loaded peptide with an association of only 22%. Hence, one could have expected a lower activity for the pre-loaded particles if only the free peptide was contributing to the bacterial killing, which was not the case. These findings indicate that the observed antimicrobial effect of the particles is not only due to the free non-encapsulated peptide. Moreover, LL-37 loaded particles which showed a very high encapsulation efficacy (80% pre-loaded and 60% as post-loaded) had a strong effect against gram negative bacteria, such as EC, but no effect on gram positive. Therefore, these findings suggest there might be a particle-bacteria interaction, also giving rise to bacterial killing. None of the reference particles displayed any antimicrobial effect in the MIC tests.

The formulations showing promising antimicrobial activity in the MIC tests were further characterized using time-kill assays with SA (Figure 12) and EC (Figure 13) bacteria. As observed in the MIC tests, formulations containing AP114 showed a similar antimicrobial effect against SA at a concentration of 16 µg/mL, compared to unformulated peptide. In case

of post-loaded AP114, 8  $\mu\text{g}/\text{mL}$  was found not to be enough for sufficient bacterial killing, as seen in Figure 12 B.

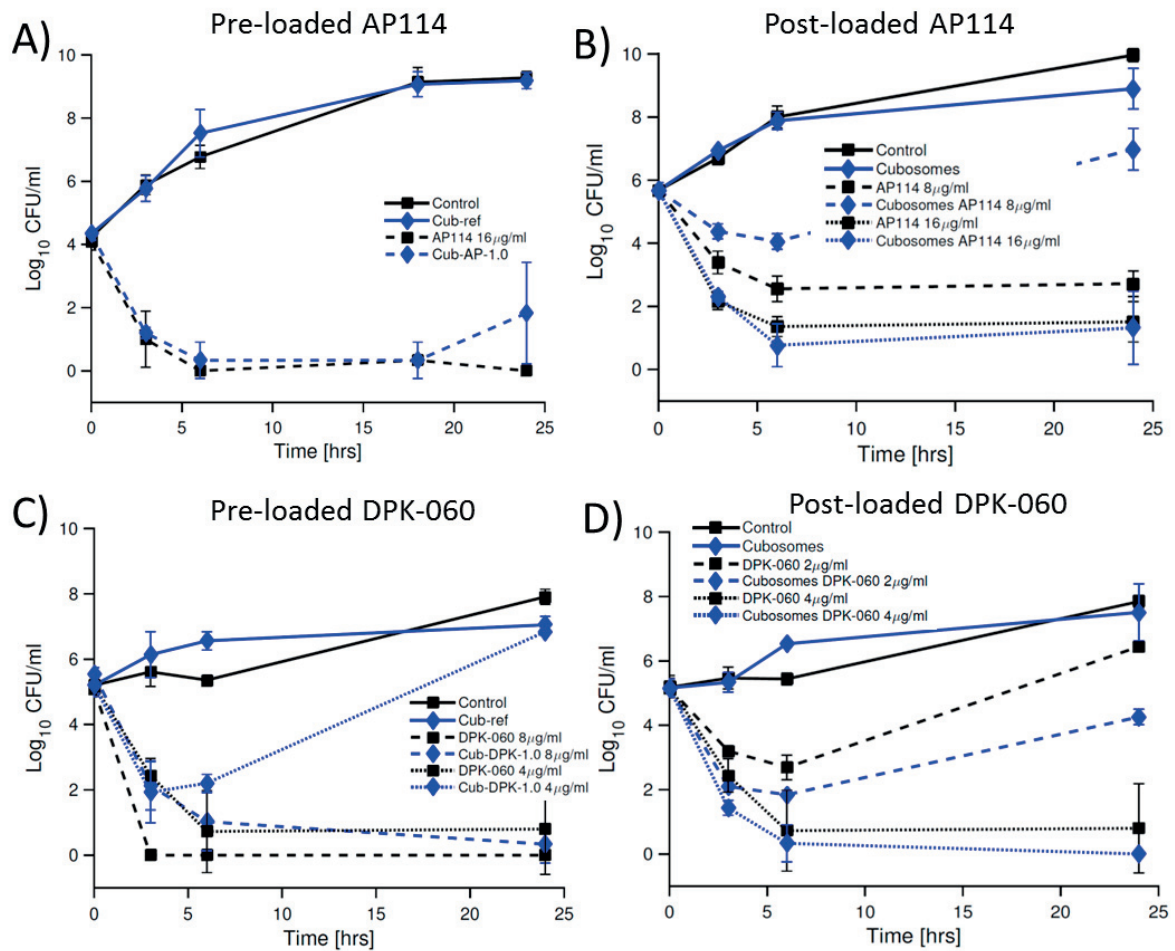


**Figure 12.** Time-kill curves for pre- and post- loaded GMO-based LCNPs containing AP114 (A and B) and DPK-060 (C and D) at selected AMP concentrations on *Staphylococcus aureus*. Each data point is represented by mean  $\pm$  standard deviation ( $n=3$ ).

Interestingly, DPK060 post-loaded LCNPs appeared to be slightly more effective against SA (Figure 12 D) and EC (Figure 13 B) strains, compared to unformulated DPK060. Post-loaded DPK-060 showed a 1-2 dilutions lower MIC on SA, and time-kill experiments confirmed a slightly more effective bacterial killing both at 2 and 4  $\mu\text{g}/\text{mL}$ . This effect can be considered synergistic, as the same trend was observed in both MIC and time-kill experiments. Pre-loaded DPK-060 and LL-37 displayed a preserved antimicrobial effect on EC (Figure 13 A and C). The 1-2 dilutions lower MIC for the DPK-060 sample on EC, could not be confirmed by the time-kill assay. The post-loaded LL-37 sample displayed a preserved activity on EC at 16  $\mu\text{g}/\text{mL}$ , but performed surprisingly better than unformulated peptide at only 4  $\mu\text{g}/\text{mL}$ . This moderate increase in activity could be contributed to the unexpected antimicrobial activity of post-loaded reference cubosomes during the first 3 hours on EC (Figure 13 B and D). The reason for this effect remains unclear as it was not observed in the MIC test. However, the pre-loaded reference particles did never display any antimicrobial effect in the time-kill assays.

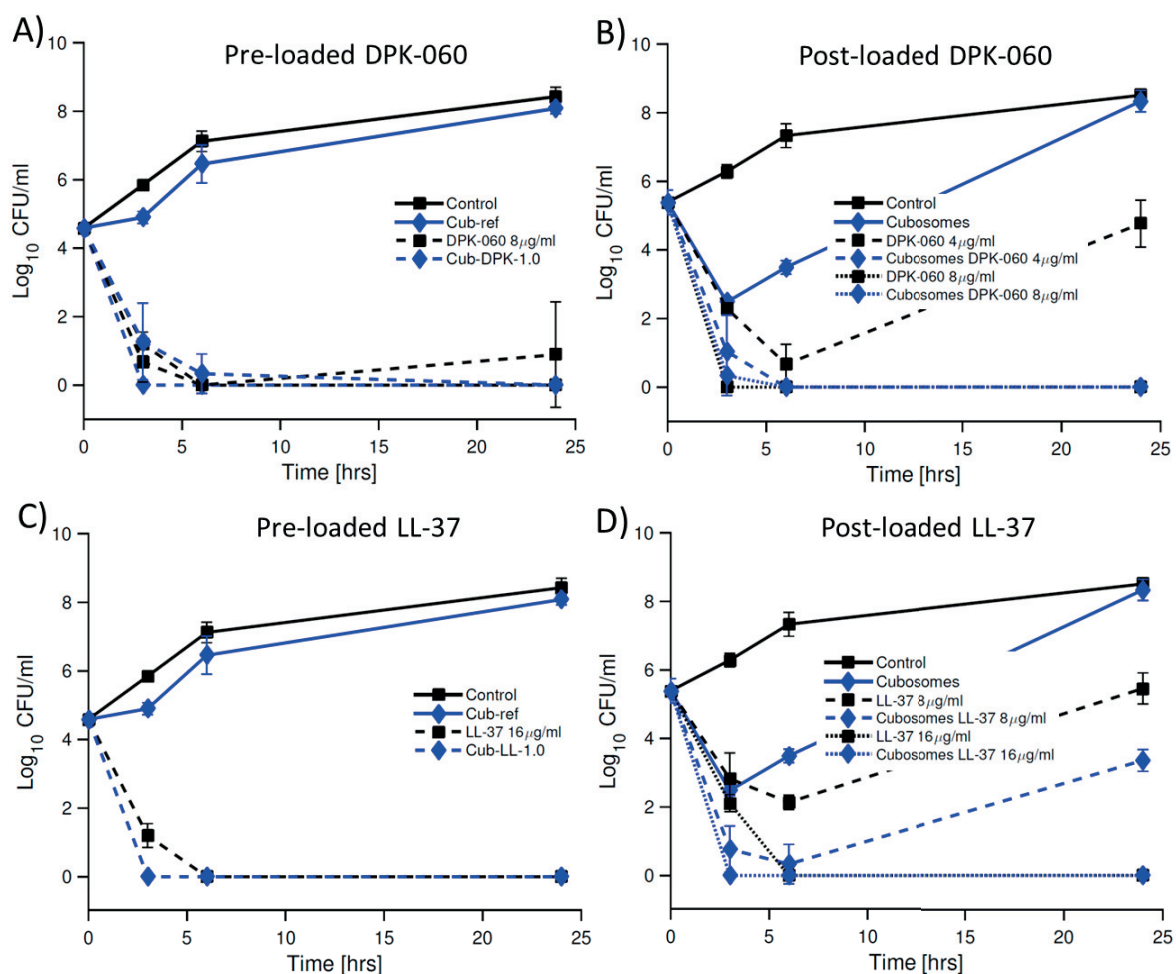


**Figure 13.** Time-kill curves for pre- and post-loaded LCNPs (GMO-based) with peptides DPK-060 (A and B) and LL-37 (C and D) at selected AMP concentrations on *Escherichia coli*. Each data point is represented by mean  $\pm$  standard deviation (n=3).

The decrease in antimicrobial activity for the pre-loaded hexagonal GMO/OA LCNPs may be explained by that peptides tend to like staying in the hexagonal environment (no phase change observed by SAXS) and are thus less prone to leak out. This may explain the high peptide loading efficacy (>94%) and will probably result in a very slow release from these particles. Our MIC data suggest that the release from the hexagonal particles is very low or non-existing during the first 24 hours. Another explanation could be the fact that the  $\zeta$ -potential of these particles always was negative (below -15 mV) giving rise to electrostatic repulsion between the particles and negatively charged bacterial membranes, thus hindering a sufficient delivery of peptide.

The release experiments might provide further insight to the in vitro antibacterial effect of the formulations. The 100% BHI and 1% BHI medium in water used for in vitro studies contains roughly the same ionic strength as the buffer, or with 150 mM NaCl, used for the release experiments. The release of AMP from the cubosomes was found to be greatest during the first 6 hours, in line with the killing kinetics shown by the time-kill assays. For a majority of the AMP loaded cubosomes, the bacterial killing reached its maximum after 6 hours incubation. If the release is as low in the 100% BHI media for AP114 as in the buffer with 150 mM NaCl

(only 30% released peptide after 24 hours), one would probably not expect such good antimicrobial effect, if not the peptide loaded particle itself will contribute to the bacterial killing. The DPK-060 loaded cubosomes displayed a very similar release as for the reference peptide in the buffer with no extra salt added. One would thus expect a very similar bacterial killing *in vitro*, which also was the case. However, the slightly synergistic effect observed for DPK-060 loaded cubosomes on SA and EC cannot be contributed to differences in release profiles. Data suggest it might instead come from a particle-bacteria interaction, giving rise to the mild increase in activity.

In order to visualize the bacterial killing and cell morphology, bacterial samples of SA were fixated and dried to enable imaging using SEM. Cells were treated in the same way as for the time-kill assay, and viewed after 10 hours incubation. Reference bacterial cells were found in large clusters, and displayed a smooth surface morphology, without any apparent damage. Moreover, the post-loaded particles on their own were found not to influence the cell morphology as expected from the MIC and time-kill experiments. Images of SA cells treated with post-loaded cubosomes containing AP114 and DPK-060, including references, are displayed in Figure 14. Both pure peptides and peptide-particle formulations displayed a drastic reduction in cell density on the glass substrates while viewed in the microscope. Bacterial cells subjected to any of the two peptides usually showed a rough surface morphology and deformations. Sometimes totally lysed (Figure 14 C) and “raisin”-like cells (Figure 14 E and F) as well as cracks and holes on the surface could be observed, in line with previously reported images of AMP treated bacteria [47-49].

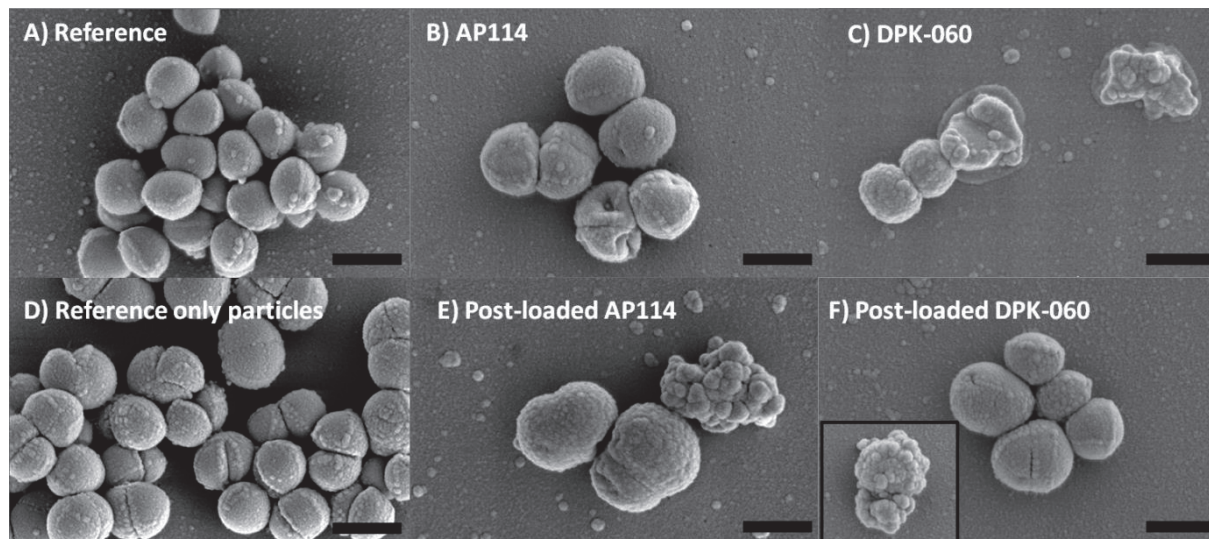


**Figure 14.** SEM images SA treated with AP114 and DPK-060 post-loaded cubosomes after 10 h incubation time. Clear cell damage is observed when the cells were subjected to any of the AMPs. Scale bar equals 1  $\mu\text{m}$ .

### 3.4. Proteolytic stability of post-loaded cubosomes

The proteolytic stability of the pure AMPs and post-loaded on cubosomes was investigated using two enzymes; *Pseudomonas aeruginosa* elastase (PE) and human neutrophil elastase (HNE). After incubation with the elastases the samples were separated by size, using gel-electrophoresis. The data is presented in Figure 15 and showed that AP114 and DPK-060 (both controls and post-loaded on cubosomes) were not degraded by any of the two enzymes. However, pure LL-37 was found to be degraded by both PE and HNE (as seen by the fuzzy bands in Figure 15 B and C), in line with data found in literature [50]. Interestingly, LL-37 post-loaded cubosomes was shown to protect the peptide against attacks from both PE and HNE. It was previously shown that the AMP melittin adsorbed onto lipid-disks particles was protected from proteolytic attacks of trypsin [51]. It was hypothesized that the polyethylene glycol (PEG) stabilizer located on the rim of the particles provided steric hindrance, blocking efficient peptide-enzyme interactions. The block copolymer PEO-PPO-PEO (P407), used as stabilizer for the cubosome particles, may protect the LL-37 peptide from enzymatic degradation in a similar way.

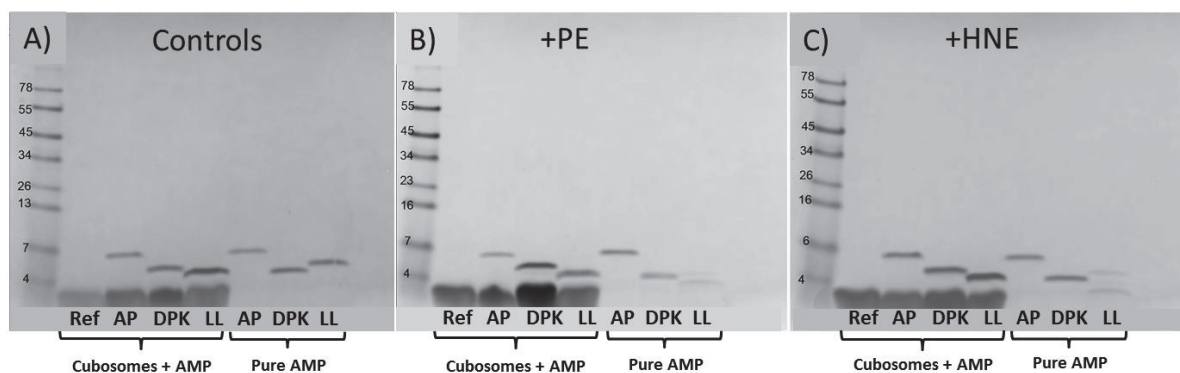


**Figure 15.** Proteolysis of post-loaded cubosomes; control samples without any enzyme (A), after 6 hours incubation with PE (B) and HNE (C). Results shows that AP114 and DPK-060 was not affected by the enzymes (strong bands), while LL-37 was degraded (fuzzy bands). LL-37 was found to be protected against the proteolytic attacks if the peptide was loaded onto cubosomes.

Radial diffusion assay (RDA) was used to investigate the antibacterial effect of post-loaded cubosomes as they were (controls) and after proteolysis with PE or HNE. The results are shown in Figure 16. As observed in the MIC-tests, it was found that pure AP114 (control) showed good bacterial killing against SA. Moreover, it was found that DPK-060 and LL-37 killed SA, PA and EC, in line with MIC and time-kill assays discussed earlier. Cubosomes post-loaded with AP114 and LL-37, without any enzyme incubation, displayed a similar effect as pure peptide. DPK-060 loaded cubosomes performed slightly poorer than pure DPK-060, a phenomenon not expected by the MIC and time-kill assays. However, the difference may be attributed to different killing mechanisms or AMP delivery mechanisms. The MIC and time-kill assays were performed on planktonic bacteria, compared to the RDA where the bacteria were fixated in an agarose gel. Hence, the bacterial killing in RDA is a result of peptide and/or particle diffusion.

Interestingly, the RDA showed a significantly better effect of LL-37 post-loaded cubosomes after exposure to PE or HNE, compared to unformulated LL-37. These observations were in line with the proteolysis data, showing that the cubosomes protected LL-37 from proteolytic degradation. Moreover, DPK-060 loaded cubosomes did maintain the peptide's broad spectrum activity after incubation with PE (SA, PA and EC) compared to unformulated peptide showing activity only against SA and PA.

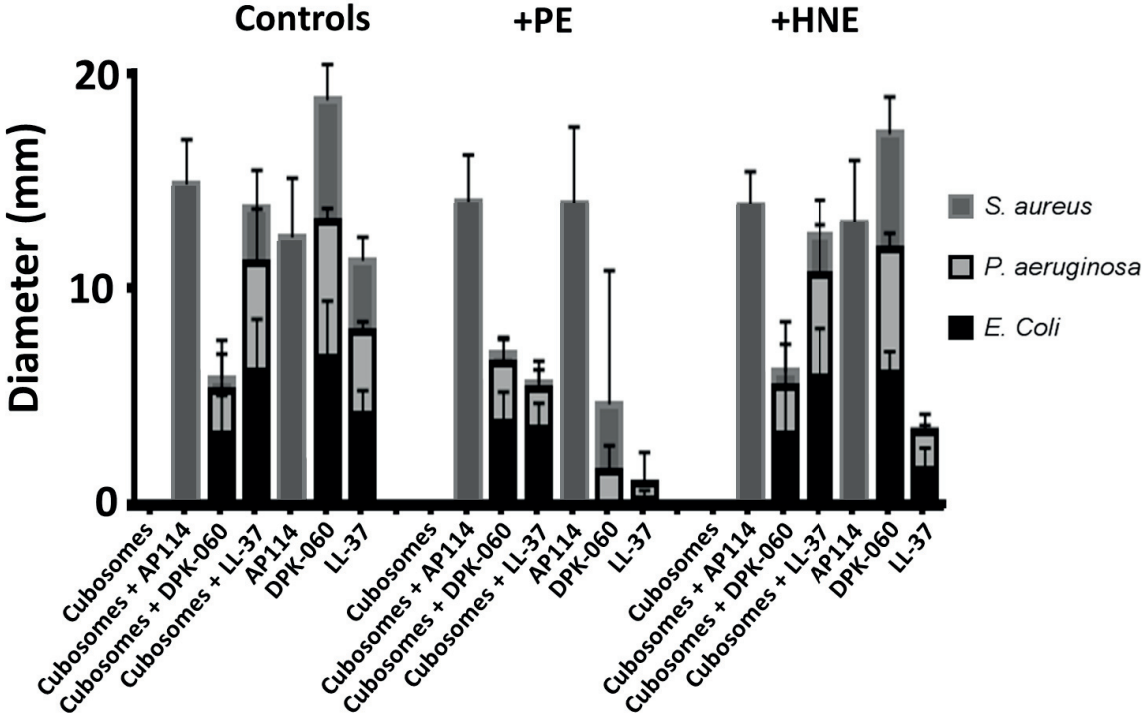


**Figure 16.** Bactericidal effect of references and post-loaded cubosomes after incubation with PE or HNE on SA, PA and EC monitored as killing around a pre-formed well in the agar gel containing bacteria. Larger diameter corresponds to more effective radial diffusion of the AMP, and in turn bacterial killing. Data is presented as mean + standard deviation (n=5 for EC, and n=4 for PA and SA).

## 4. Conclusions

As the number of multi drug resistant bacteria constantly increases around the globe, the demand for novel antibiotics and efficient treatment strategies is rising. AMPs have recently received a great attention in the scientific community, but adequate drug delivery systems for these peptides are still needed, in order to reach the clinic.

In this thesis, we have demonstrated that AMPs could successfully be loaded in cubic and hexagonal LC gels, and in LCNPs using two different peptide loading strategies; pre- and post-loading. The main findings are summarized in Table 3. It was demonstrated that the AMPs strongly influenced the LC structure of the cubic GMO/water system. The net charge and degree of hydrophobicity of the AMPs were found to be important factors, affecting the curvature of the LC system, but also the loading efficacy of the LCNPs. However, the hexagonal GMO/OA/water gel kept its hexagonal structure upon peptide incorporation. The hexagonal LCNPs were found to be very efficient in encapsulating the AMPs, but did not display any antimicrobial effect, indicating insufficient delivery of peptide to the bacteria.

Importantly, the cubic pre- and post-loaded LCNPs showed promising antimicrobial activity, and sometimes could a synergetic effect be observed, resulting in a slightly better activity than the unformulated AMP. This was the case of post-loaded DPK-060, showing encouraging bacterial killing against SA and EC strains. Moreover, it was shown that LL-37 post-loaded onto cubosomes did protect the peptide from enzymatic degradation and that the presence of cubosomes enhanced the bactericidal effect after proteolysis. Steric hindrance from the particle stabilizer (P407) may inhibit a sufficient enzyme-peptide interaction, providing protection of the peptide.

**Table 3.** Summary of the main conclusions of this thesis.

<b>System</b>	<b>Cubosome</b>	<b>Cubosome</b>	<b>Hexosome</b>
<b>AMP loading strategy</b>	<b>pre</b>	<b>post</b>	<b>pre</b>
<b>Lipid composition</b>	GMO	GMO	GMO/OA
<b>AMP loading efficacy</b>	moderate	poor/moderate	excellent
<b>Particle uniformity</b>	good	excellent	moderate
<b>Antimicrobial activity</b>	good	good	poor
<b>Proteolytic protection</b>	*	good	*
<b>Antibacterial effect after proteolysis</b>	*	good	*

\*Not yet investigated

## 5. Future perspectives

So far, we have demonstrated that LCNPs could be used as drug delivery vehicles for AMPs. However, the reason for the differences in antimicrobial activity between pre-loaded cubosomes and hexosomes remains unclear and could be further investigated. Is it an insufficient release of peptide or a weaker interaction of the hexosomes with the bacterial cells? The high encapsulation efficacy for the hexosomes could be favorable giving rise to an effective proteolytic protection, which has so far not been investigated.

In case of pre- and post-loaded cubosomes the mechanism of delivery of peptide is an interesting topic to study. Does the cubosome particle fuse together with the bacterial membrane and delivers the peptide? Model bacterial membrane interactions studies using quartz crystal microbalance with dissipation monitoring (QCM-D), ellipsometry or neutron reflectivity could provide hints about these questions. Moreover, fluorescently marked peptides and particles could be used together with fluorescent microscopy techniques to study the interaction with live bacterial cells.

## 6. References

1. Pierson, E., D.T. Hung, and A.E. Clatworthy, *Targeting virulence: a new paradigm for antimicrobial therapy*. Nature Chemical Biology, 2007. **3**(9): p. 541-548.
2. WHO, *Antimicrobial resistance: global report on surveillance*. 2014.
3. Pasupuleti, M., A. Schmidtchen, and M. Malmsten, *Antimicrobial peptides: key components of the innate immune system*. Critical reviews in biotechnology, 2012. **32**(2): p. 143-171.
4. Hancock, R.E.W. and H.-G. Sahl, *Antimicrobial and host-defense peptides as new anti-infective therapeutic strategies*. Nature biotechnology, 2006. **24**(12): p. 1551-1557.
5. Eckert, R., *Road to clinical efficacy: challenges and novel strategies for antimicrobial peptide development*. Future Microbiology, 2011. **6**(6): p. 635-651.
6. Andersson, D.I., D. Hughes, and J.Z. Kubicek-Sutherland, *Mechanisms and consequences of bacterial resistance to antimicrobial peptides*. Drug Resistance Updates, 2016. **26**: p. 43-57.
7. Hancock, R.E.W. and R. Lehrer, *Cationic peptides: a new source of antibiotics*. Trends in Biotechnology, 1998. **16**(2): p. 82-88.
8. Schneider, T., T. Kruse, R. Wimmer, I. Wiedemann, V. Sass, U. Pag, A. Jansen, A.K. Nielsen, P.H. Mygind, D.S. Raventós, S. Neve, B. Ravn, M.J.J.B. Alexandre, L.D. Maria, A.S. Andersen, L. Gammelgaard, H.-G. Sahl, and H.-H. Kristensen, *Plectasin, a Fungal Defensin, Targets the Bacterial Cell Wall Precursor Lipid II*. Science, 2010. **328**(5982): p. 1168-1172.
9. Fischer, R.L., K.M. Schnorr, H.-H. Kristensen, D. Yaver, C.P. Sönksen, S.G. Elvig-Jørgensen, B. Christensen, B.E. Christensen, R.I. Lehrer, N. Frimodt-Møller, S. Ludvigsen, L. De Maria, D. Raventós, P.H. Mygind, S. Kjærulff, S. Buskov, M.T. Hansen, M.V. Sørensen, M. Zasloff, and O. Taboureau, *Plectasin is a peptide antibiotic with therapeutic potential from a saprophytic fungus*. Nature, 2005. **437**(7061): p. 975-980.
10. Schmidtchen, A., M. Pasupuleti, M. Mörgelin, M. Davoudi, J. Alenfall, A. Chalupka, and M. Malmsten, *Boosting Antimicrobial Peptides by Hydrophobic Oligopeptide End Tags*. Journal of Biological Chemistry, 2009. **284**(26): p. 17584-17594.
11. Dürr, U.H.N., U.S. Sudheendra, and A. Ramamoorthy, *LL-37, the only human member of the cathelicidin family of antimicrobial peptides*. BBA - Biomembranes, 2006. **1758**(9): p. 1408-1425.
12. Strömstedt, A.A., M. Pasupuleti, A. Schmidtchen, and M. Malmsten, *Evaluation of Strategies for Improving Proteolytic Resistance of Antimicrobial Peptides by Using Variants of EFK17, an Internal Segment of LL-37*. Antimicrobial Agents and Chemotherapy, 2009. **53**(2): p. 593-602.
13. Milak, S. and A. Zimmer, *Glycerol monooleate liquid crystalline phases used in drug delivery systems*. International Journal of Pharmaceutics, 2015. **478**(2): p. 569-587.
14. Chen, Y., P. Ma, and S. Gui, *Cubic and Hexagonal Liquid Crystals as Drug Delivery Systems*. BioMed Research International, 2014.
15. Qiu, H. and M. Caffrey, *The phase diagram of the monoolein/water system: metastability and equilibrium aspects*. Biomaterials, 2000. **21**(3): p. 223-234.
16. Caboi, F., G.S. Amico, P. Pitzalis, M. Monduzzi, T. Nylander, and K. Larsson, *Addition of hydrophilic and lipophilic compounds of biological relevance to the monoolein/water system. I. Phase behavior*. Chemistry and Physics of Lipids, 2001. **109**(1): p. 47-62.

17. Borné, J., T. Nylander, and A. Khan, *Phase Behavior and Aggregate Formation for the Aqueous Monoolein System Mixed with Sodium Oleate and Oleic Acid*. Langmuir, 2001. **17**(25): p. 7742-7751.
18. Salentinig, S., L. Sagalowicz, and O. Glatter, *Self-Assembled Structures and pKa Value of Oleic Acid in Systems of Biological Relevance*. Langmuir, 2010. **26**(14): p. 11670-11679.
19. Angelova, A., R. Ionov, M.H.J. Koch, and G. Rapp, *Interaction of the Peptide Antibiotic Alamethicin with Bilayer- and Non-bilayer-Forming Lipids: Influence of Increasing Alamethicin Concentration on the Lipids Supramolecular Structures*. Archives of Biochemistry and Biophysics, 2000. **378**(1): p. 93-106.
20. Angelova, A., B. Angelov, B. Papahadjopoulos-Sternberg, M. Ollivon, and C. Bourgaux, *Proteocubosomes: Nanoporous Vehicles with Tertiary Organized Fluid Interfaces*. Langmuir, 2005. **21**(9): p. 4138-4143.
21. Angelova, A., B. Angelov, B. Papahadjopoulos-Sternberg, M. Ollivon, and C. Bourgaux, *Structural organization of proteocubosome carriers involving medium- and large-size proteins*. Journal of Drug Delivery Science and Technology, 2005. **15**(1): p. 108-112.
22. Angelova, A., B. Angelov, S. Lesieur, R. Mutafchieva, M. Ollivon, C. Bourgaux, R. Willumeit, and P. Couvreur, *Dynamic control of nanofluidic channels in protein drug delivery vehicles*. Journal of Drug Delivery Science and Technology, 2008. **18**(1): p. 41-45.
23. Angelov, B., A. Angelova, B. Papahadjopoulos-Sternberg, S.V. Hoffmann, V. Nicolas, and S. Lesieur, *Protein-Containing PEGylated Cubosomic Particles: Freeze-Fracture Electron Microscopy and Synchrotron Radiation Circular Dichroism Study*. The Journal of Physical Chemistry B, 2012. **116**(26): p. 7676-7686.
24. Angelova, A., B. Angelov, M. Drechsler, V.M. Garamus, and S. Lesieur, *Protein entrapment in PEGylated lipid nanoparticles*. International Journal of Pharmaceutics, 2013. **454**(2): p. 625-632.
25. Angelov, B., A. Angelova, S.K. Filippov, M. Drechsler, P. Štěpánek, and S. Lesieur, *Multicompartment Lipid Cubic Nanoparticles with High Protein Upload: Millisecond Dynamics of Formation*. ACS Nano, 2014. **8**(5): p. 5216-5226.
26. Larsson, K., *Cubic lipid-water phases: structures and biomembrane aspects*. The Journal of Physical Chemistry, 1989. **93**(21): p. 7304-7314.
27. Gustafsson, J., H. Ljusberg-Wahren, M. Almgren, and K. Larsson, *Cubic Lipid–Water Phase Dispersed into Submicron Particles*. Langmuir, 1996. **12**(20): p. 4611-4613.
28. Rizwan, S.B., B.J. Boyd, T. Rades, and S. Hook, *Bicontinuous cubic liquid crystals as sustained delivery systems for peptides and proteins*. Expert Opinion on Drug Delivery, 2010. **7**(10): p. 1133-1144.
29. Shah, J.C., Y. Sadhale, and D.M. Chilukuri, *Cubic phase gels as drug delivery systems*. Advanced Drug Delivery Reviews, 2001. **47**(2–3): p. 229-250.
30. Angelova, A., B. Angelov, R. Mutafchieva, S. Lesieur, and P. Couvreur, *Self-Assembled Multicompartment Liquid Crystalline Lipid Carriers for Protein, Peptide, and Nucleic Acid Drug Delivery*. Accounts of Chemical Research, 2010. **44**(2): p. 147-156.
31. Gustafsson, J., H. Ljusberg-Wahren, M. Almgren, and K. Larsson, *Submicron Particles of Reversed Lipid Phases in Water Stabilized by a Nonionic Amphiphilic Polymer*. Langmuir, 1997. **13**(26): p. 6964-6971.
32. Spicer, P.T., K.L. Hayden, M.L. Lynch, A. Ofori-Boateng, and J.L. Burns, *Novel Process for Producing Cubic Liquid Crystalline Nanoparticles (Cubosomes)*. Langmuir, 2001. **17**(19): p. 5748-5756.

33. Barauskas, J., M. Johnsson, F. Joabsson, and F. Tiberg, *Cubic Phase Nanoparticles (Cubosome<sup>†</sup>): Principles for Controlling Size, Structure, and Stability*. Langmuir, 2005. **21**(6): p. 2569-2577.
34. Chung, H., J. Kim, J.Y. Um, I.C. Kwon, and S.Y. Jeong, *Self-assembled "nanocubicle" as a carrier for peroral insulin delivery*. Diabetologia, 2002. **45**(3): p. 448-451.
35. Rizwan, S.B., D. Assmus, A. Boehnke, T. Hanley, B.J. Boyd, T. Rades, and S. Hook, *Preparation of phytantriol cubosomes by solvent precursor dilution for the delivery of protein vaccines*. European Journal of Pharmaceutics and Biopharmaceutics, 2011. **79**(1): p. 15-22.
36. Gordon, S., K. Young, R. Wilson, S. Rizwan, R. Kemp, T. Rades, and S. Hook, *Chitosan hydrogels containing liposomes and cubosomes as particulate sustained release vaccine delivery systems*. Journal of Liposome Research, 2012. **22**(3): p. 193-204.
37. Rattanapak, T., K. Young, T. Rades, and S. Hook, *Comparative study of liposomes, transfersomes, ethosomes and cubosomes for transcutaneous immunisation: characterisation and in vitro skin penetration*. Journal of Pharmacy and Pharmacology, 2012. **64**(11): p. 1560-1569.
38. Cervin, C., P. Vandoolaeghe, C. Nistor, F. Tiberg, and M. Johnsson, *A combined in vitro and in vivo study on the interactions between somatostatin and lipid-based liquid crystalline drug carriers and bilayers*. European Journal of Pharmaceutical Sciences, 2009. **36**(4-5): p. 377-385.
39. Lopes, L., D. Ferreira, D. Paula, M.T. Garcia, J. Thomazini, M.A. Fantini, and M.V.B. Bentley, *Reverse Hexagonal Phase Nanodispersion of Monoolein and Oleic Acid for Topical Delivery of Peptides: in Vitro and in Vivo Skin Penetration of Cyclosporin A*. Pharmaceutical Research, 2006. **23**(6): p. 1332-1342.
40. Lai, J., Y. Lu, Z. Yin, F. Hu, and W. Wu, *Pharmacokinetics and enhanced oral bioavailability in beagle dogs of cyclosporine A encapsulated in glyceryl monooleate/poloxamer 407 cubic nanoparticles*. International journal of nanomedicine, 2010. **5**: p. 13-23.
41. Labrador, A., Y. Cerenius, C. Svensson, K. Theodor, and T. Plivelic, *The yellow mini-hutch for SAXS experiments at MAX IV Laboratory*. Journal of Physics: Conference Series, 2013. **425**(7): p. 072019.
42. Hyde, S.T., *Identification of Lyotropic Liquid crystalline Mesophases*, in *Handbook of Applied Surface and Colloid Chemistry*, K. Holmberg, Editor. 2001, John Wiley & Sons, Ltd. p. 299-332.
43. Böhlen, P., S. Stein, W. Dairman, and S. Udenfriend, *Fluorometric assay of proteins in the nanogram range*. Archives of Biochemistry and Biophysics, 1973. **155**(1): p. 213-220.
44. Briggs, J., H. Chung, and M. Caffrey, *The temperature-composition phase diagram and mesophase structure characterization of the monoolein/water system*. Journal de Physique II, 1996. **6**(5): p. 723-751.
45. Yaghmur, A., P. Laggner, S. Zhang, and M. Rappolt, *Tuning curvature and stability of monoolein bilayers by designer lipid-like peptide surfactants*. PloS one, 2007. **2**(5): p. e479.
46. Johansson, J., G.H. Gudmundsson, M.E. Rottenberg, K.D. Berndt, and B. Agerberth, *Conformation-dependent antibacterial activity of the naturally occurring human peptide LL-37*. J Biol Chem, 1998. **273**(6): p. 3718-24.
47. Valcourt, C., P. Saulnier, A. Umerska, M.P. Zanelli, A. Montagu, E. Rossines, and M.L. Joly-Guillou, *Synergistic interactions between doxycycline and terpenic*

- components of essential oils encapsulated within lipid nanocapsules against gram negative bacteria.* International journal of pharmaceutics, 2016. **498**(1-2): p. 23-31.
48. Hartmann, M., M. Berditsch, J. Hawecker, M.F. Ardakani, D. Gerthsen, and A.S. Ulrich, *Damage of the Bacterial Cell Envelope by Antimicrobial Peptides Gramicidin S and PGLa as Revealed by Transmission and Scanning Electron Microscopy.* Antimicrobial Agents and Chemotherapy, 2010. **54**(8): p. 3132-3142.
49. Kasetty, G., M. Kalle, M. Mörgelin, J.C. Brune, and A. Schmidtchen, *Anti-endotoxic and antibacterial effects of a dermal substitute coated with host defense peptides.* Biomaterials, 2015. **53**: p. 415-425.
50. Braun, K., A. Pochert, M. Lindén, M. Davoudi, A. Schmidtchen, R. Nordström, and M. Malmsten, *Membrane interactions of mesoporous silica nanoparticles as carriers of antimicrobial peptides.* Journal of Colloid and Interface Science, 2016. **475**: p. 161-170.
51. Zetterberg, M.M., K. Reijmar, M. Pránting, Å. Engström, D.I. Andersson, and K. Edwards, *PEG-stabilized lipid disks as carriers for amphiphilic antimicrobial peptides.* Journal of Controlled Release, 2011. **156**(3): p. 323-328.